CHEMISTRY OF MATERIALS
Cite This: Chem. Mater. 2019, 31, 4657−4672
Article
pubs.acs.org/cm

Spontaneous Microalgae Dewatering Directed by Retrievable, Recyclable, and Reusable Nanoparticle-Pinched Polymer Brushes

Liangju Kuang,[†,#] Jason Goins,[‡] Wan Zheng,[⊥] Patrick Eduafo,[‡] Hairong Ma,[⊥] Matthew Posewitz,[‡] David T. Wu,[‡,§] and Hongjun Liang*[,∥,⊥]

[†]Department of Metallurgical and Materials Engineering, [‡]Department of Chemistry, and [§]Department of Chemical and Biological Engineering, Colorado School of Mines, Golden, Colorado 80401, United States

[∥]Departments of Chemical Engineering and Chemistry, Texas Tech University, Lubbock, Texas 79409, United States

[⊥]Department of Cell Physiology and Molecular Biophysics, Texas Tech University Health Sciences Center, Lubbock, Texas 79430, United States

Supporting Information

ABSTRACT: Selective capture and separation of solution−borne planktonic cells is a ubiquitous challenge in diverse fields ranging from biofilm mitigation, cancer diagnostics, and water treatment to microalgae biofuels. Microalgae are promising feedstocks for carbon-neutral biofuels that will alleviate our repentant dependency on fossil fuels, but current technologies for dewatering microalgae add a prohibitive cost to the final products. We report here a nanoparticle-pinched polymer brush (NPPB) design that transforms ordinary polymer flocculants into supercoagulants by mimicking bacterial outer membrane vesicles in promoting bacteria coaggregation. Importantly, the NPPBs are retrievable via cost-effective magnetophoretic separation, recyclable after algae oil extraction and residual biomass removal, and reusable for repeated cycles of operations that significantly reduces the endless material cost of flocculants and their potential contamination of downstream processes and the environment. Using DLVO and self-consistent field theory to model the colloidal stability of microalgae and the dynamic response of polymer brushes, respectively, we reveal a fundamental transition from conventional chain-like polymer flocculants to NPPBs in modulating the interalgae pair potentials. Unlike the chain-like polymer flocculants that only induce slow microalgae dewatering with dose-sensitive flocculation-dissociation equilibria, NPPBs direct rapid and irreversible microalgae coagulation. Although a minimum brush size on the NPPBs is predicted to initiate the coagulation, the benefit of increasing brush size quickly wanes and there is an optimal brush size beyond which the coagulation efficiency plateaus, which is consistent with our experimental observations. We anticipate that the concept of retrievable, recyclable, and reusable NPPBs is adaptable for capturing a broad range of live cells in solution.

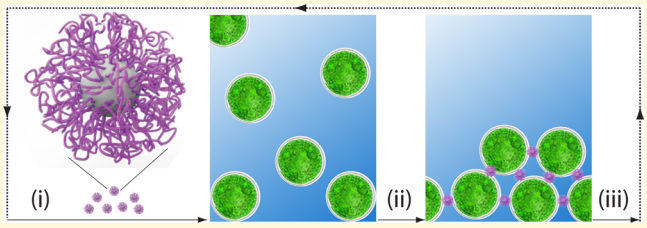

Fossil fuels provide nearly two-thirds of the electricity; 92% of the transportation fuels and 81% of all energy consumed in the United States.[1,2] They are the ultimate commodity on which virtually our entire polymer and pharmaceutical industries are built.[3] A world without fossil fuels is unthinkable in the foreseeable future, but our continued reliance on fossil fuels is unsustainable because of their depleting supplies and the alarming accumulation of greenhouse gases due to their consumption. Microalgae-derived biofuels have been actively pursued as renewable and carbon-neutral fuels for decades.[4−7] Since the Department of Energy's Landmark Aquatic Species Program in 1978,[8] enormous progress has been made on algal species collection, metabolic engineering, algaculture module development, and conversion of algal biomass into biofuels.[9−14] In contrast, the technology for microalgae dewatering, that is, the separation of algal cells from their dilute growth media (∼0.01 wt %), remains essentially the same as what was known 40 years ago.[15−17] Sedimentation, centrifugation, flocculation, flotation, and filtration are the methods of choice,[15−17] whereas alternatives based on ultrasound standing waves[18,19] and magnetic particles[20−24] have gained increasing attention in recent years. Notwithstanding the great promise of microalgae, various economic analyses have suggested that the current technologies for microalgae dewatering add a huge cost to the final products[15−17,25−28] and present "a major bottleneck to algae-based fuels".[15]

From a broader perspective, selective capture and separation of solution−borne planktonic cells are a ubiquitous challenge in diverse fields ranging from water treatment,[29] biofilm mitigation,[30] metastatic cancer diagnostics,[31] to microalgae biofuels.[15−17] Microalgae present a simple model to test the underlying principles governing live cell dispersion and aggregation in the solution. A microalgae culture can be best described as a dilute colloidal solution of live cells with a

Received: January 24, 2019
Revised: May 31, 2019
Published: June 3, 2019

DOI: 10.1021/acs.chemmater.9b00336
Chem. Mater. 2019, 31, 4657−4672

typical cell volume fraction of 10^{-3} or lower, such that solution-mediated interalgae pair potentials strongly influence their phase behavior. Similar to many other solution−borne planktonic cells, their intrinsic stability comes from their low cell number density, small cell sizes, like-charge repulsions, and low specific gravity (especially for those microalgae strains with high oil content). Current technologies for microalgae dewatering are conveniently borrowed from either laboratory-scale operations (e.g., centrifugation and ultrasonic sedimentation) or industrial practices of water and mineral processing (e.g., filtration, flocculation, and flotation).[15−17,32−34] Centrifugation and ultrasonic sedimentation are inevitably small-scale batch processes with high-energy inputs and operational costs;[11,15−18] filtration is subject to clogging and short running times, hence accompanied by high energy, labor, and material costs;[5,32−34] flotation is not only slow and inefficient but also introduces complications to downstream processes because of the frequent use of surfactants;[35−37] chemical flocculation applies either pro-oxidants to liberate extracellular substances[38] or electrolytes (e.g., polymers or small cations) to screen the surface charges of microalgae[39−48] in order to aid cell-to-cell adhesion. To achieve optimal efficiency, the pH of algal growth media is often adjusted to a specific range and a high dose of flocculants needs to be applied. For instance, the mass ratio of polymer flocculants to fresh-water microalgae can reach ∼1:1,[15,41] and this ratio may rise 5−10 times further for marine microalgae because of their high-medium salinity.[15,42] The need to change pH and the endless cost of flocculants are incompatible with large-scale operations. Also, both flotation and chemical flocculation need additional energy-intensive separations to collect the slowly settled algal biomass, and the chemicals used in both approaches introduce problematic contamination to post-dewatering algaculture or biofuel conversion.[37,45] None of the current microalgae dewatering technologies suits biofuel production with desirable energy efficiency, harvesting efficiency, and compatibility to downstream processing. This deficiency highlights the knowledge gap underlying the phase separation of live cells in the solution.

We aim to address this deficiency and gap of knowledge by the development of retrievable, recyclable, and reusable nanoparticle-pinched polymer brushes (NPPBs) that direct microalgae dewatering spontaneously. We reason that the interalgae pair potentials can be fine-tuned with well-defined polymer brushes that are tethered onto the cell surfaces but stretch out away from the surface far exceeding the Debye length,[49] a critical distance beyond which the electrostatic repulsion between two like-charge bodies (e.g., anionic algal cells) in the solution decays significantly. We report here the proof-of-concept design of NPPB[50] (Figure 1) that transforms ordinary polymer flocculants into supercoagulants. Each NPPB is composed of three components (Figure 1a): a paramagnetic Fe_3O_4 nanoparticle core, a silica shell that not only protects the Fe_3O_4 core from degrading but also opens up rich silane chemistry for surface modifications, and a "hairy" outer layer consisting of covalently grafted polymer brushes. As a model system, we grow well-defined poly(4-vinylpyridine) (P4VP) brushes on the silica shell via surface-initiated atom transfer radical polymerization (SI-ATRP). The resultant NPPBs (i.e., Fe_3O_4@SiO_2@P4VP) reveal clearly their triple-layer structure under transmission electron microscopy (TEM). As an example, a TEM picture of Fe_3O_4@SiO_2@$P4VP_{347}$, where 347 denotes the P4VP degree of polymerization (DP), is shown (Figure 1b). The P4VP is subsequently converted to cationic poly(4-vinyl-*N*-methylpyridine iodide) (P4MVP) via a quaternization reaction[51] to interact with anionic algal cells. Although any cationic polymer brushes bearing quaternary amine pendant groups might be used in the model system, the stability of P4MVP over some cationic polymers (e.g., methacrylate[52]) is an advantage for recycling and reusing NPPBs.

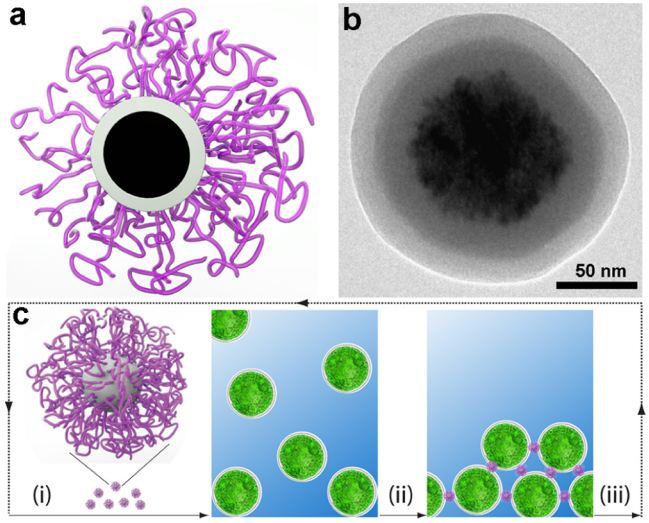

Figure 1. Retrievable, recyclable, and reusable NPPBs for cost-effective microalgae dewatering. (a) Cross-sectional illustration of the NPPB design consisting of a paramagnetic nanoparticle core (black) encased by a silica shell (gray) with covalently grafted polyelectrolyte brushes (purple) on the outer surface. (b) Example TEM picture of NPPB (scale bar: 50 nm). The paramagnetic Fe_3O_4 core (black), SiO_2 shell (gray), and P4VP brush outer layer (light gray) are clearly shown because of their different electron densities. (c) Schematic diagram of NPPB-directed microalgae dewatering cycles: (i) cationic NPPBs (purple "hairy" balls) are added into a culture of microalgae (green spheres); (ii) spontaneous microalgae dewatering ensues, and the coagulated algal biomass precipitates out; and (iii) algal biomass is retrieved magnetophoretically and subjected to algal oil extraction and residual biomass removal. The recovered NPPBs are directly reused for algae dewatering.

Unlike other cationic polymer flocculants carrying primary, secondary, or tertiary amines,[39−47] the NPPBs carry quaternary ammoniums on their P4MVP brushes and remain cationic regardless of solution pH. Once attached to algal cells, a solid-state nanoparticle can provide a guaranteed intercell spacing greater than the Debye length. The stretching P4MVP brushes sitting on the opposite surface of the nanoparticle will bridge neighboring cells without suffering an otherwise overwhelming penalty of interalgae repulsions. This mode of action differs fundamentally from chain-like polymer flocculants that are adhered to the algal cell surface at multiple sites along their chains,[39,40,53,54] such that the suspending chain loops or dangling chain ends are often too short to interact with neighboring cells that are kept apart by their like-charge repulsions. Our strategy of using NPPBs as the coagulation mediators mimics how biology directs live cell coaggregation: planktonic bacteria staying apart in solution due to like-charge repulsions are known to secrete outer membrane vesicles (typical diameters ≈ 25−150 nm) with functionally displayed, multivalent adhesions to promote homologous and heterologous bacteria coagulation, a key step for biofilm formation.[55,56]

DOI: 10.1021/acs.chemmater.9b00336
Chem. Mater. 2019, 31, 4657−4672

EXPERIMENTAL SECTION

Synthesis and Characterization of NPPBs. Experimental details on the synthesis and characterization of NPPBs are described in the Supporting Information. The size and size distribution of nanoparticles were analyzed by TEM (Philips CM200) and ImageJ (NIH, Bethesda, MD). The radii of Fe_3O_4 and Fe_3O_4@SiO_2 nanoparticles are r = 80.9 ± 15.4 and 99.0 ± 18.1 nm, respectively, whereas those of NPPBs vary depending on their brush sizes.

Fourier Transform Infrared Spectroscopy. Attenuated total reflection−Fourier-transform infrared spectroscopy (FT-IR) spectra were collected using a Thermo Electron Corporation Nicolet 4700 FT-IR Spectrometer System coupled with a smart SAGA accessory. The grafting content (x) of P4VP on NPPBs was evaluated using its characteristic adsorption at 1595 cm^{-1} as a reference to compare with an internal standard, that is, the Si−O−Si adsorption of silica at 1091 cm^{-1}, using eq 1

$$x = \left(\frac{A_{(P4VP)}}{A_{(SiO_2)}}\right) \times 100\% \tag{1}$$

where $A_{(P4VP)}$ and $A_{(SiO_2)}$ are the areas of the two peaks, respectively, calculated using the Thermo OMNIC software by selecting the same band ranges of SiO_2 and P4VP peaks, respectively, on each individual spectrum of NPPBs to ensure consistent and reliable comparison. Similar method that uses FT-IR to quantitatively compare the grafted polymer contents has also been reported elsewhere.[57]

The Si−O−Si adsorption at 1091 cm^{-1} was chosen as the internal standard because it is the commonly shared and only dominated peak in the band range of 1280−980 cm^{-1} used to determine the $A_{(SiO_2)}$ of individual NPPBs. Because P4VP also has weak adsorption peaks in this range, we first measured the FT-IR of free P4VP to determine the areas of those peaks relative to the characteristic pyridyl peak at 1595 cm^{-1}, $\alpha = A_{(P4VP,1280-980)}/A_{(P4VP,1595)}$. We then eliminated the contribution of P4VP brushes from individual NPPBs to their $A_{(SiO_2)}$ by calculating $A_{(SiO_2)} = A_{(SiO_2,1290-980)} - \alpha A_{(P4VP)}$.

The degree of quaternization (y) was also evaluated by FT-IR following a similar method using eq 2

$$y = \left(1 - \frac{A_{t(P4VP)}}{A_{t(SiO_2)}} \Big/ \frac{A_{0(P4VP)}}{A_{0(SiO_2)}}\right) \times 100\% \tag{2}$$

where A_0 and A_t represent the peak areas before and after quaternization, respectively. We used both NMR and FT-IR to determine the quaternization of P4VP before[58] and verified that FT-IR is a reliable method for this analysis.

Thermal Gravimetric Analysis. We used the thermal gravimetric analysis (TGA) 2950 thermogravimetric analyzer to measure the weight percentage loss (w) of the ATRP initiator or P4VP grafted on unit mass of nanoparticles. The samples were heated from room temperature to 500 °C under N_2 protection at a heating rate of 10 °C/min. The grafting density (σ) was calculated using eq 3

$$\sigma = \left(w \cdot \frac{N}{M}\right)/S \tag{3}$$

where N is Avogadro's number, M is the molecular weight of the grafted moiety (i.e., ATRP initiator or P4VP), and S is the average specific surface area of ATRP-initiator-modified nanoparticles (i.e., Fe_3O_4@SiO_2@Br) or NPPBs.

The weight percentage loss (w) of ATRP initiator or P4VP brushes was calculated according to eq 4

$$w = w_2 - w_1 \tag{4}$$

When we calculate the grafting density of the ATRP initiator, w_1 and w_2 refer to the weight percentage losses of 3-aminopropyltriethoxysilane (APTES)-modified nanoparticles (i.e., Fe_3O_4@SiO_2@NH_2) and Fe_3O_4@SiO_2@Br, respectively, and M is 149 Da, that is, the molecular weight of the grafted ATRP initiator moiety on the Fe_3O_4@SiO_2@NH_2; when we calculate the grafting density of P4VP, w_1 and w_2 refer to the weight percentage losses of Fe_3O_4@SiO_2@Br and NPPBs, respectively, and M is the number-average molecular weight of P4VP brushes determined by gel permeation chromatography (GPC).

The average specific surface area (S) of Fe_3O_4@SiO_2@Br or NPPBs was calculated using eq 5

$$S = 4\pi r_2^2(1 - w_i)/\left\{\frac{4}{3}\pi[(r_2^3 - r_1^3)\rho_{SiO_2} + r_1^3\rho_{Fe_3O_4}]\right\} \tag{5}$$

where w_i is the weight percentage loss of Fe_3O_4@SiO_2@Br or NPPBs, respectively, r_1 and r_2 represent the average radii of the Fe_3O_4 (r_1 = 80.9 nm) and Fe_3O_4@SiO_2 (r_2 = 99.0 nm) nanoparticles, respectively, and ρ is the density of Fe_3O_4 ($\rho_{Fe_3O_4}$ = 5.17 g/mL) or SiO_2 (ρ_{SiO_2} = 1.90 g/mL). Our TGA analysis to calculate graft density is conceptually similar to that reported in other polymer brush systems.[52]

Transmission Electron Microscopy. We also calculated the grafting density of P4VP (σ) directly by measuring its thickness on individual NPPBs, assuming that the P4VP layer is a condensed solid shell because of the vacuum environment under TEM. Our TEM analysis to calculate graft density is conceptually similar to that reported in other polymer brush systems.[52,59]

The average grafting density σ was obtained from many individual measurements (n > 30) using eq 6

$$\sigma = (\rho V_{P4VP} N)/(M S_{(Fe_3O_4@SiO_2)}) \tag{6}$$

where ρ is the P4VP density (1.114 g/cm^3),[60] V_{P4VP} is the volume of the P4VP brush layer, N is Avogadro's number, M is the number-average molecular weight of P4VP brushes determined by GPC, and $S_{(Fe_3O_4@SiO_2)}$ is the surface area of individual Fe_3O_4@SiO_2. The V_{P4VP} and $S_{(Fe_3O_4@SiO_2)}$ were calculated using eqs 7 and 8, respectively

$$V_{P4VP} = \frac{4}{3}\pi(r_3^3 - r_2^3) \tag{7}$$

$$S_{(Fe_3O_4@SiO_2)} = 4\pi r_2^2 \tag{8}$$

where r_2 and r_3 represent the radii of individual Fe_3O_4@SiO_2 and NPPBs, respectively.

We further used cross-sectional TEM to study the NPPB-directed microalgae dewatering. The microalgae were cultured and dewatered as described in the sections below. The free algal cells used as controls were collected by centrifugation of the algae culture at 1000g for 5 min. The harvested algal cells were fixed in 2.5% glutaraldehyde in the growth medium for 24 h, then washed with the growth medium three times to remove the excess glutaraldehyde, post-fixed with 1% osmium tetraoxide (OsO_4) for 1 h, and followed by three additional washes with the growth medium to remove the excess OsO_4. After a series of dehydration with 25, 50, 75, and 100% of ethanol, the fixed algal cells were infiltrated with a solution of LX112 resin/acetone (weight ratio 1/2) for 2 h. The LX112 resin consists of LX112, dodecenyl succinic anhydride, and nadic methyl anhydride at a mass ratio of 1.8/1/0.9. An accelerator DMP-30 (2,4,6-tris-(dimethylaminomethyl)phenol) was added to the resin mixture (1% v/v) right before use. The fixed algal cells were further infiltrated with LX112 resin/acetone = 1/1 and 2/1 solutions for 2 h, respectively, and embedded in 100% LX112 resin and incubated at 65 °C for 2 days. The solidified resin block was cut into pieces of ∼80 nm thickness with an ultramicrotome (Reichert-Jung Ultracut E) equipped with a diamond blade. The as-cut pieces were stained with 4% uranyl acetate and Reynolds' lead citrate and then placed on 200 mesh copper grids for imaging using the Hitachi H-8100 TEM equipped with an AMT digital side mount camera.

Scanning Electron Microscopy. We also used scanning electron microscopy (SEM) to study the NPPB-directed microalgae dewatering. The harvested algal cells were fixed by glutaraldehyde as described above, followed by dehydration using a series of ethanol washes (25, 50, 75, and 100%) and lyophilized in the Labconco freeze dryer (Kansas City, MO). The fixed and dried algal cells were placed

DOI: 10.1021/acs.chemmater.9b00336
Chem. Mater. 2019, 31, 4657−4672

on a carbon tape mounted on an aluminum stud and then coated with a thin layer of gold prior to SEM analysis using the JEOL JSM7000F field emission SEM (Peabody, MA) with an accelerating voltage of 10 kV and a medium probe current.

Microalgae. Both fresh-water and marine microalgae were used as models to test our NPPB design. Fresh-water *Chlamydomonas reinhardtii* (CC-124 wild type mt-[137c]; hereafter referred as "C.r.") was purchased from Chlamydomonas Resource Center (St. Paul, MN). Marine *Nannochloropsis gaditana* (CCMP 526; hereafter referred as "N.g.") was obtained from the National Center for Marine Algae and Microbiota (NCMA). The C.r. was cultured for 5 days with a starting concentration of ∼0.2 mg/mL in a Tris/acetate/phosphate medium at pH 7.2, and the N.g. was cultured for 15 days with a starting concentration of ∼0.5 mg/mL in an artificial seawater medium, both in Erlenmeyer flasks on a rotary shaker at a speed of 125 rpm and under a fluorescent light intensity of ∼100 μmol m^{-2} s^{-1}.

Harvesting Efficiency. The microalgae harvesting (or dewatering) efficiency of cationic NPPBs was measured and compared to that of Fe_3O_4, Fe_3O_4@SiO_2, and free P4MVP chains. We standardize our dewatering tests as follows: the dry cell weight (DCW) density of microalgae was adjusted to 1 mg/mL, and the concentration of coagulant stocks was set at 5 mg/mL. The DCW was determined by either centrifugation (for C.r.) or filtration (for N.g.) of the microalgae culture using a 0.7 μm glass fiber filter (Pall Corporation, Port Washington, NY), followed by washing the algal biomass with deionized water and vacuum-drying overnight at 80 °C. In each 20 mL transparent glass vial containing 15 mL of algal culture, a defined dose of coagulant was quickly added by a pipette and mixed thoroughly for 2 min. The vials with nanoparticles were subsequently placed side-by-side to a magnet for 2 more min. This particular magnet position was chosen to minimize the effect of gravity. The vial with free P4MVP was simply allowed to settle during this time. We confirmed that the sedimentation of both C.r. and N.g. without coagulation agents was negligible in 2 min and all nanoparticles were precipitated out by the magnet after the 2 min interaction. To determine algae concentration, 3 samples at ∼1/3, 1/2, and 2/3 solution height in individual vials were pipetted out and each sample was repeated in triplicate. The harvesting efficiency (HE) was calculated by eq 9, in which the optical density (OD) of C.r. and N.g. was measured at 699 and 690 nm, respectively, with a UV−vis spectrophotometer (Agilent Technologies, Santa Clara, CA)

$$\mathrm{HE} = (\mathrm{OD_i} \times V_i - \mathrm{OD_f} \times V_f)/(\mathrm{OD_i} \times V_i) \times 100\% \quad (9)$$

where $\mathrm{OD_i}$, $\mathrm{OD_f}$, V_i, and V_f are initial and final OD, and initial and final volumes of the algal solutions, respectively.

Adsorption Isotherm. Adsorption isotherms depict the correlation between adsorbate on a substrate and free adsorbate in the solution. They reveal the adsorption capacity of a flocculant on microalgae and help to elucidate the mechanism of coagulation. The Langmuir model is used to describe monolayer adsorption, whereas the Freundlich model is valid for either monolayer or multilayer adsorption on heterogeneous surfaces possessing different adsorption sites or energies.[61,62] The Langmuir isotherm model can be expressed as

$$\frac{C_e}{Q_e} = \frac{1}{Q_m K_L} + \frac{C_e}{Q_m} \quad (10)$$

where C_e (mg/mL) is the concentration of free microalgae in the solution, Q_e (mg/mg-particles) is the mass of microalgae adsorbed onto unit mass of nanoparticles, Q_m (mg/mg-particles) is the maximum adsorption capacity for monolayer coverage, and K_L (mL/mg) is the Langmuir constant related to the energy of adsorption.

The Freundlich isotherm model is shown in eq 11

$$\log Q_e = \log K_F + \frac{1}{n} \log C_e \quad (11)$$

where K_F (mg/mg-particles) and $1/n$ are the Freundlich constant related to the adsorption capacity and the exponent of nonlinearity, respectively.

To determine the adsorption isotherms between microalgae and cationic NPPBs, we first constructed the calibration curves between the DCW density and the OD of both microalgae using a series of cultures at different concentrations. The linear calibration curves were determined as: $\mathrm{DCW_{C.r.}}$ (mg/mL) = $0.148\mathrm{OD_{699}} - 0.0490$, R^2 = 0.998; and $\mathrm{DCW_{N.g.}}$ (mg/mL) = $0.180\mathrm{OD_{690}} - 0.0158$, R^2 = 0.997. Note that in different growth phases, variations in algal biological activities may lead to changes in chlorophyll concentrations; therefore, this linear relationship may vary slightly. To minimize errors, we constructed the calibration curves with the same batch of microalgae used for the coagulation experiments. Cationic NPPBs Fe_3O_4@SiO_2@$P4MVP_{245}$ and Fe_3O_4@SiO_2@$P4MVP_{198}$ at concentrations of 0.0288 and 0.150 mg/mL, respectively, were used for C.r. (DCW density at 0.13, 0.21, 0.32, 0.42, 0.51, 0.59, 0.68, 0.77, 0.97, 1.04, and 1.26 mg/mL) and N.g. (DCW density at 0.56, 0.74, 0.96, 1.15, 1.37, 1.55, 1.74, 2.02, 2.13, and 2.73 mg/mL).

Retrieve and Reuse Magnetic Nanoparticles. After dewatering microalgae with Fe_3O_4, Fe_3O_4@SiO_2, or cationic NPPBs, the nanoparticle−algae flocs were first treated with methanol/chloroform (v/v = 2/1) and hexanes to extract the algal oil and then dried in a vacuum oven at 40 °C. The remaining nanoparticle−algae biomass was subsequently dispersed in 100-fold (mass ratio) ionic liquid 1-butyl-3-methylimidazoliumchloride ([BMIM]Cl) in the Schlenk line. The mixture was degassed by three freeze−pump−thaw cycles and treated at 110 °C overnight. Attention should be taken to keep water and oxygen away from the mixture as they may cause degradation of the nanoparticles at this temperature. After dissolving all residual algal biomass, the nanoparticles were retrieved by a magnet and washed with methanol. The structural integrity of the recycled nanoparticles was verified by zeta potential, dynamic light scattering (DLS), FT-IR, and TEM studies. The reusability of recycled nanoparticles was assessed by measuring their dewatering efficiency.

Reuse of the Microalgae Culture Medium. To test the reusability of the algal growth medium for repeated cycles of algaculture, the supernatant was collected after magnetophoretic separation of the coagulated algal biomass. The essential nutrients (NO_3^-, PO_4^{3-}, acetic acid, and trace elements) were restored. Microalgae were regrown under the aforementioned conditions, and the algal cell number density was monitored to compare the growth profiles.

Computation and Modeling. Methods and approaches to model NPPB-directed spontaneous microalgae dewatering are discussed in the Supporting Information.

Other Characterizations. Optical pictures of the algal cells and flocs were acquired using a Nikon Eclipse E800 microscope. The chemical structures of all polymers were characterized using a JEOL 500 MHz NMR spectrometer with $CDCl_3$ or DMSO-d_6 as a solvent. Their molecular weight was measured by GPC (Viscotek model 270 series platform) in DMF at a flow rate of 1.0 mL/min, using the Visco Gel I-series G-3000 and G-4000 mixed bed columns (molecular weight range 0 to 20×10^3 and 0 to 200×10^3 g/mol, respectively). The GPC is a triple detector system coupled with a Viscotek differential viscometer, a low-angle laser light scattering detector (model 270, λ = 670 nm, 3 mW laser, detector angles positioned at 7° and 90°, respectively), and a refractive index detector model 3580 (10 mV, λ = 660 nm). The DLS size and the zeta potential of the nanoparticles were measured by the Malvern Instruments Zetasizer Nano ZS90. The different hydrodynamic radii of Fe_3O_4@SiO_2 and Fe_3O_4@SiO_2@P4MVP in the aqueous solution as measured by DLS were used to determine the P4MVP brush lengths. The algal cell number density was assessed using a Z2 Coulter Counter cell and particle counter (Beckman−Coulter, Brea, CA). Algal cells were assumed to be spherically shaped, and cellular debris was excluded in all cellular count, volume, and diameter assessments.

Statistical Analysis. All experiments were conducted at least three times unless otherwise mentioned. Differences among groups were assessed by two-tailed unpaired *t*-tests to identify statistical

DOI: 10.1021/acs.chemmater.9b00336
Chem. Mater. 2019, 31, 4657−4672

differences. A p-value of 0.05 was set as the criterion for statistical significance. Data are presented as mean ± standard deviation.

RESULTS AND DISCUSSION

Synthesis and Characterization of NPPBs with Well-Controlled Brush Sizes. Elemental analysis of the ATRP initiator-modified nanoparticles Fe_3O_4@SiO_2@Br revealed the weight percentage of bromine to be 0.43%, suggesting that a grafting density of the initiator is 4.0/nm^2. In corroboration of that, TGA showed an extra weight loss of 0.83% between the Fe_3O_4@SiO_2@NH_2 and Fe_3O_4@SiO_2@Br nanoparticles, suggesting a grafting density of 4.2/nm^2. We prepared model NPPBs with well-controlled brush lengths using SI-ATRP. Example pictures of Fe_3O_4 nanoparticles (black) and cationic NPPBs (brown) in water are shown in Figure S1 (Supporting Information). CuCl/$CuCl_2$/Me_6TREN was selected as the catalyst to slow down the rate of propagation with respect to initiation and to increase the stability of the dormant species toward nucleophilic substitution by limiting competitive complexation of the 4VP or P4VP to Cu(I). Kinetic study of the growth of P4VP brushes on Fe_3O_4@SiO_2@Br in the presence of free initiator, 2-(EtBi)−Br, was conducted. As shown in the lower panel of Figure 2a, a first-order kinetics between the monomer consumption and reaction time indicates a constant free-radical concentration during the polymerization. A linear increase of the molecular weights of the free P4VP in solution was also observed (Table 1), indicating that the number of propagating species remains constant. The polydispersity indices (PDIs), that is, the ratios between the weight- and number-average molecular weight of the free P4VP, remained low ($M_w/M_n \approx 1.1-1.2$) throughout the polymerization (Figure 2a, top panel), indicating that the growth of P4VP was well defined and characteristic of a controlled/"living" polymerization process. We expect that the chain length of free P4VP grown in the solution is the same as the brush length of P4VP grown simultaneously on the nanoparticles because it is well recognized that in the synthesis of polymer brushes on nanoparticles via controlled/"living" polymerization, little difference exists between the surface-bound polymer chains and that grown in the solution.[63−66] Just for reassurance, we cleaved the P4VP brushes from the NPPBs and compared them with the free P4VP concurrently grown in the solution, as an example shown in Figure S2. We confirmed that, within experimental errors, both P4VP chains have similar molecular weight, suggesting that the same chain propagation process occurs simultaneously in solution and on the nanoparticles. We did observe a larger PDI for the P4VP cleaved from NPPBs, likely because of possible intermolecular branching or cross-linking between adjacent P4VP brushes.[67] Nevertheless, those events have a little effect on the P4VP brush lengths estimated from the DP of free P4VP in the solution.

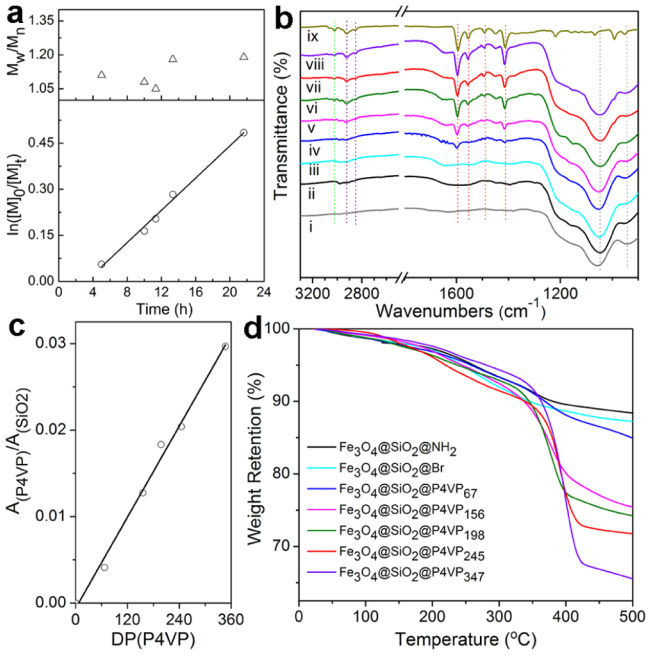

Figure 2. Synthesis of model NPPBs with well-defined brush sizes via SI-ATRP. (a) Both the first-order kinetic plot (bottom panel) and small PDIs of P4VP in the solution (top panel) suggest a controlled/"living" polymerization process. $[M]_0$ and $[M]_t$ refers to the 4VP concentration at time 0 and t, respectively. (b) FT-IR comparison of (i) Fe_3O_4@SiO_2, (ii) Fe_3O_4@SiO_2@NH_2, (iii) Fe_3O_4@SiO_2@Br, (ix) free P4VP, and NPPBs with increasing P4VP brush sizes (i.e., DP) at (iv) 67, (v) 156, (vi) 198, (vii) 245, and (viii) 347, respectively. (c) Quantitative analysis of the P4VP brushes on NPPBs by their normalized FT-IR absorption peaks shows that the amount of surface-grafted P4VP increases linearly with the DP of free P4VP in the solution. (d) TGA comparison of nanoparticles before and after the growth of P4VP brushes with different brush lengths.

The controlled/"living" polymerization of P4VP brushes on nanoparticles was further confirmed by FT-IR (Figure 2b,c) and TGA (Figure 2d). The absorption peaks of nanoparticles at 1091 and 952 cm^{-1} (marked by dotted gray lines) are attributed to the Si−O−Si vibration and Si−OH stretching modes, respectively. The reduction of the band at 952 cm^{-1} for traces (ii−viii) as compared to trace (i) points to the successful surface modifications on the Fe_3O_4@SiO_2 nanoparticles (Figure 2b). Because of the presence of P4VP brushes, FT-IR spectra of NPPBs [i.e., traces (iv−viii)] show new peaks at 1595, 1553, 1447, and 1412 cm^{-1} (marked by dotted red lines) characteristic of pyridyl ring stretching vibrations, a new peak at 3022 cm^{-1} (marked by dotted green line) attributed to asymmetric stretching of pyridyl −C−H and increased absorption at 2920 and 2850 cm^{-1} (marked by dotted purple lines) because of aliphatic −C−H stretching. The attribution of these peaks is further confirmed by their presence in free P4VP (ix) and their absence in nanoparticles before P4VP grafting (i−iii). The content of P4VP on NPPBs was analyzed by normalizing its characteristic peak at 1595 cm^{-1} against the internal standard, that is, SiO_2 adsorption at 1091 cm^{-1}. This ratio increases linearly with the sizes of free P4VP in the solution (Figure 2c), again suggesting that both surface-bound and free P4VP in the solution grow at the same pace, and a constant free-radical concentration persists during polymerization.

TGA also revealed the well-defined nature of P4VP brushes on NPPBs, with increasing percentage weight loss when the DP of P4VP increased (Figure 2d). The weight loss below ∼100 °C was assigned mainly to the loss of adsorbed water and other solvents, whereas that between ∼300 and 450 °C was attributed to the degradation of P4VP. The weight losses of APTES and initiator moieties were hidden in the background because of their small contributions, but we expect that they ended before 450 °C similar to the P4VP. Besides these organic moieties, condensation and cross-linking within the SiO_2 shell, which led to the additional loss of H_2O,

DOI: 10.1021/acs.chemmater.9b00336
Chem. Mater. 2019, 31, 4657−4672

Table 1. Summary of the Structural Characterization Data for the Model NPPBs

NPPBs	M_n (g/mol)[a]	PDI[a]	P4VP thickness (nm)[b]	grafting density (nm^{-2})[b]	grafting density (nm^{-2})[c]
Fe_3O_4@SiO_2@P4VP$_{67}$	7 000	1.11	4.4 ± 0.6	0.44 ± 0.06	0.54
Fe_3O_4@SiO_2@P4VP$_{156}$	16 400	1.08	10.4 ± 1.8	0.48 ± 0.11	0.60
Fe_3O_4@SiO_2@P4VP$_{198}$	20 760	1.05	14.7 ± 1.9	0.55 ± 0.09	0.61
Fe_3O_4@SiO_2@P4VP$_{245}$	26 000	1.18	17.6 ± 3.1	0.54 ± 0.13	0.61
Fe_3O_4@SiO_2@P4VP$_{347}$	36 500	1.19	26.5 ± 6.0	0.59 ± 0.14	0.64

[a]Determined by GPC analysis of free P4VP in the solution. [b]Determined by TEM analysis. [c]Determined by TGA analysis.

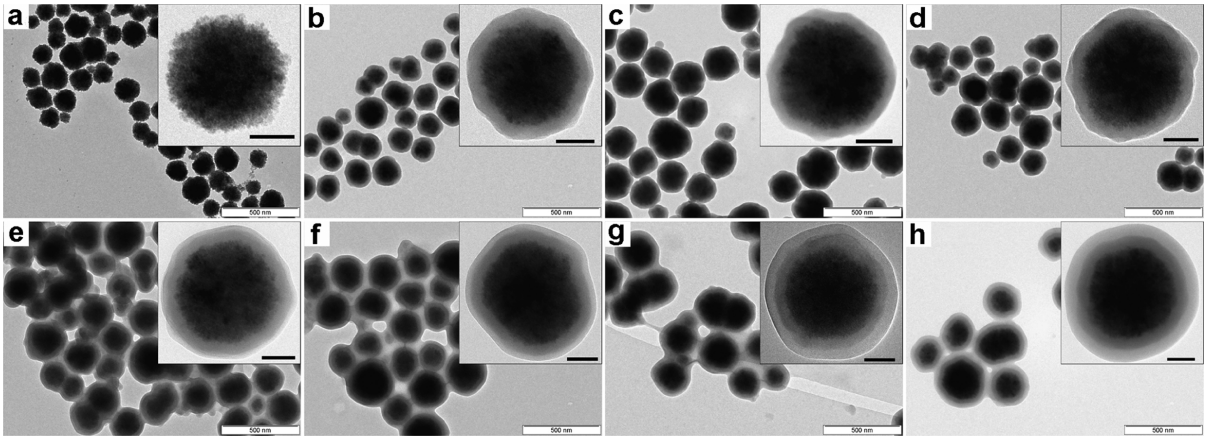

Figure 3. TEM pictures of nanoparticles (scale bar: 500 nm). (a) Fe_3O_4, (b) Fe_3O_4@SiO_2, (c) Fe_3O_4@SiO_2@NH_2, and NPPBs with increasing P4VP brush lengths, (d) DP = 67, (e) DP = 156, (f) DP = 198, (g) DP = 245, and (h) DP = 347, respectively. Insets: Representative individual nanoparticles (scale bar: 50 nm).

are expected to run continuously up to 500 °C and beyond.[66] To minimize systematic errors, we used the difference in weight percentage losses between Fe_3O_4@SiO_2@Br and Fe_3O_4@SiO_2@NH_2 and that between Fe_3O_4@SiO_2@Br and NPPBs, respectively, to calculate the grafting density of ATRP initiator and P4VP brushes. Our TGA showed that most NPPBs have fairly close P4VP grafting density around 0.60 ± 0.06 nm^{-2} (Table 1).

Because the typical interfacial area per polymer chain is ~2.5 nm^2,[68] the measured grafting density suggests that the P4VP brushes were closely packed and approaching the maximum possible occupancy. As such, when the P4VP brush length increases, an increasingly thicker P4VP layer is expected, which can be directly seen under TEM and analyzed to infer the grafting density. This is exactly what was observed (Figure 3). The Fe_3O_4 nanoparticles by themselves appear as black nanospheres with radii r = 80.9 ± 15.4 nm (panel a). After coating with silica, a core−shell structure where the black Fe_3O_4 core encased by a less electron-dense, a gray silica shell is apparent (panel b) and the radii of individual nanoparticles increase to 99.0 ± 18.1 nm. Further modifying Fe_3O_4@SiO_2 with APTES does not alter its appearance (panel c), but a third light gray layer starts to show up when P4VP brushes are covalently grown on the surface of Fe_3O_4@SiO_2 (panels d−h). Initially, this polymer layer is thin and barely discernible when the DP of P4VP is small (DP = 67, panel d), but it expands as expected when the P4VP brush length increases (panel e−h), corroborating the well-defined nature of our model polymer brushes as demonstrated in FT-IR, TGA, and kinetics studies (Figure 2). For each brush length, we analyzed many individual NPPBs (n > 30) to obtain their average P4VP layer thickness, which clearly expands with increasing P4VP brush length (Table 1). Given the particle size variations among NPPBs, we chose to calculate the P4VP grafting density on individual nanoparticles by taking direct measurement of the radius of their Fe_3O_4 cores and thickness of their SiO_2 and P4VP shells (eqs 6−8). The average grafting density derived from individual calculations is summarized in Table 1 and compared with that obtained from TGA. The two sets of grafting density data agree with each other surprisingly well; only a slightly greater deviation (~20%) occurs at small P4VP brush sizes, likely because of the difficulty to accurately measure the thickness of thin P4VP layers on the Fe_3O_4@SiO_2 with nanoscale roughness. Nevertheless, the closely matched grafting densities from the direct TEM analysis again confirm that the NPPBs have well defined and systematically varied polymer brushes, which will help test the underlying principles governing the phase separation of solution−borne live cells.

Finally, we used the quaternization reaction[51] to convert model NPPBs into their cationic forms. The 100% conversion of P4VP to P4MVP brushes is confirmed by the FT-IR analysis: the four characteristic pyridyl bands all shifted to higher pyridinium frequencies at 1639, 1571, 1516, and 1470 cm^{-1} (Figure S3a), and quantitative analysis (eq 2) confirmed the degree of quaternization is 100%. Additionally, the areas of characteristic pyridinium adsorption at 1639 cm^{-1} normalized by the internal standard also scaled linearly with the brush sizes (Figure S3b), just as that was found for the P4VP brushes (Figure 2c).

Spontaneous Microalgae Dewatering Directed by Cationic NPPBs. We chose two model microalgae, C.r. and N.g., respectively, to represent fresh-water and marine algae species. Both microalgae are favorable candidates for biofuel production, as both can accumulate ~40−50% DCW of lipid contents under special growth conditions.[69,70] The algal cells are always anionic, although their surface charges vary depending on the growth phases and media (Figure S4a,b). It is worth noting that although magnetic particles without

DOI: 10.1021/acs.chemmater.9b00336
Chem. Mater. 2019, 31, 4657−4672

surface-bound P4MVP brushes have been tested for microalgae dewatering,[20−24] their efficiency is highly dependent on pH and the dragging forces created by external magnetic fields because these particles can be either cationic or anionic depending on pH. For example, the isoelectric point of Fe_3O_4@SiO_2 is ∼3.5 (Figure S4c); it is thus always anionic in the algae growth media and repulsive to algal cells. In contrast, cationic NPPBs are always cationic regardless of pH (Figure S4d), so they will induce spontaneous microalgae dewatering in all growth media.

Besides facilitating adhesion among solution−borne live cells, NPPBs offer several additional advantages relevant to microalgae dewatering. Compared to polymer flocculants that undergo adsorption−desorption equilibrium with algal cells,[47] the cationic NPPBs cling to microalgae irreversibly because of the physically confined, high-charge-density polymer brushes. Once attached, the NPPB−algae flocs readily precipitate from algal growth media because of the high specific gravity of NPPBs. This is in sharp contrast to polymer−algae flocs that have a specific gravity close to water, such that they stay afloat in the growth media for prolonged period of time and become re-dissociated upon continuing adsorption of the polymer flocculants.[39,40]

Additionally, the paramagnetic property of NPPBs enables cost-effective magnetophoretic separation of the algae flocs without energy-intensive processes such as centrifugation or filtration. Although magnetite particles by themselves or those coated with SiO_2 have long been tested for microalgae dewatering,[20−24] their working mechanisms differ from NPPBs and have little to do with reducing the repulsive interalgal pair potentials. Because the typical pH of algal cultures is above the isoelectric point of either Fe_3O_4 (i.e., ∼6−7) or SiO_2 (i.e., ∼2−3),[71] these particles are not expected to bridge anionic algal cells electrostatically.[22] In fact, the harvesting efficiency of these particles depends on the magnetic field strength, a caveat for reducing cost.

As shown in Figure S5 and Video M1 (Supporting Information), adding cationic NPPBs into algae cultures triggered rapid phase separation of the solution into coagulated algal biomass and supernatant, and the biomass was easily harvested with a magnet. In contrast, only a small fraction of algal cells was harvested by Fe_3O_4@SiO_2 using the same magnet and significant algal cells remained afloat even after prolonged sedimentation (i.e., 3 h) when linear-chain P4MVP was used.

Optical microscopy revealed that the well-dispersed, water-borne algal cells were precipitated rapidly into closely packed algal biomass after adding the cationic NPPBs, in which "dots" of NPPBs packed at the intercellular boundaries were seen (Figure 4a,b). SEM studies further revealed the morphological difference of algal cells before and after interacting with the cationic NPPBs: the well-dispersed, water-borne algal cells (Figure 4c) were aggregated into clusters in the presence of NPPBs, and the spherical cationic NPPBs that clung to the surface of algal cells were clearly seen (Figure 4d). To elucidate the role of NPPBs on directing spontaneous microalgae dewatering, we compared the cross-sectional TEM of algal cells before and after the coagulation. Unlike free microalgae that stay away from each other due to the like-charge repulsion (Figure 4e), the dewatered algal cells clustered to each other via the interfacial NPPBs that bridged them together (Figure 4f) just as we expected. Considering the previous report about the uptake of iron oxide nanoparticles (diameter 20−30 nm)

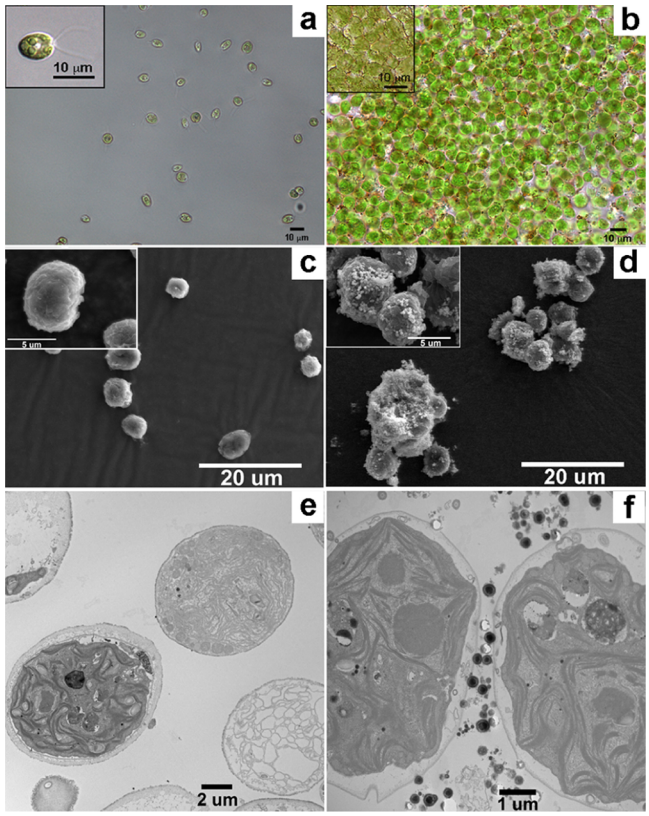

Figure 4. Spontaneous microalgae dewatering directed by cationic NPPBs. Optical microscope pictures (scale bar: 10 μm) show (a) well-dispersed C.r. in its growth medium (1 mg/mL) and (b) coagulated C.r. after adding Fe_3O_4@SiO_2@$P4MVP_{198}$. Close-up views of individual and coagulated C.r. are shown as insets. SEM studies further revealed the morphological difference of C.r. before (c) and after interacting with the cationic NPPBs (d). The well-dispersed C.r. (c) aggregate into clusters (d) in the presence of NPPBs, where the spherical NPPBs that cling to the C.r. surface are clearly seen in the close-up views [insets in (d) as compared to (c). Scale bar: 5 μm]. The role of NPPBs on directing microalgae dewatering is on full display in the cross-sectional TEM pictures of C.r. before (e) and after coagulation (f), where the water-borne algal cells staying apart because of like-charge repulsion in the absence of NPPBs (e) cluster together via the interfacial NPPBs (i.e., nanoparticles with the characteristic core−shell structures) that act as bridges (f).

by algal cells during the magnetophoretic separation process,[72] we carefully examined many cross-sectional TEM pictures of dewatered microalgae but failed to confirm the internalization of NPPBs. This difference might be due to the size difference between the two types of nanoparticles.

Our standardized dewatering tests allowed us to quantitatively compare the harvesting efficiency of model NPPBs with bare Fe_3O_4@SiO_2 and linear-chain P4MVP controls. As shown in Figure 5a,b, there is an apparent dose-dependent harvesting efficiency: the efficiency increased linearly with the dosages of cationic NPPBs before it plateaued approaching 100%, and this increase was faster for the NPPBs of longer brushes than those of shorter ones. As such, it took the NPPBs of shorter brushes higher doses to reach the same harvesting efficiency, but the difference receded at increasing brush lengths. Our observation suggests that some finite number of cationic NPPBs is needed on the surface of algal cells to overcome their like-charge repulsions. The longer the brushes, the larger the NPPBs

DOI: 10.1021/acs.chemmater.9b00336
Chem. Mater. 2019, 31, 4657−4672

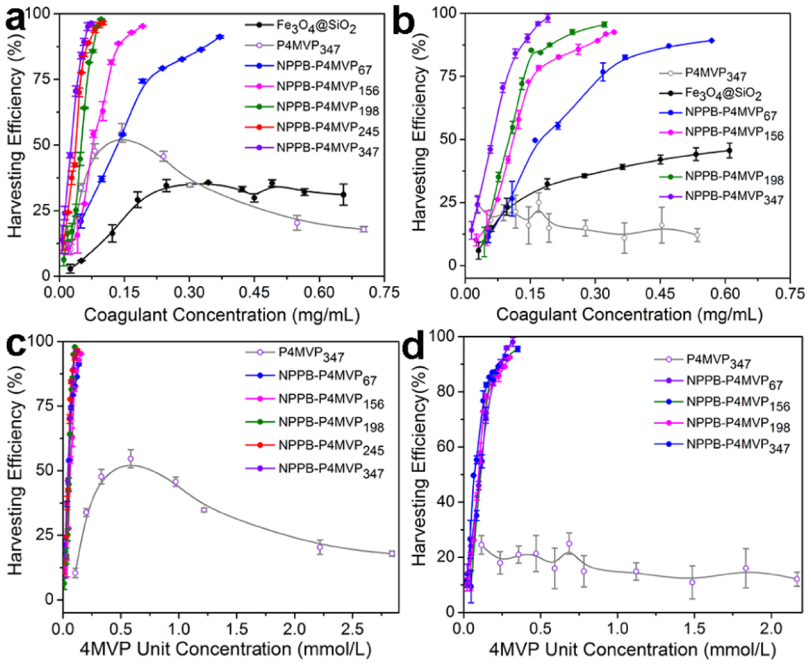

Figure 5. Comparison of the harvesting efficiency of cationic NPPBs, Fe_3O_4@SiO_2, and linear-chain P4MVP on different microalgae. The dose-dependent harvesting efficiency of (a) C.r. and (b) N.g. by the cationic NPPBs of different brush sizes is compared with bare Fe_3O_4@SiO_2 and linear-chain $P4MVP_{347}$. The doses of cationic NPPBs and $P4MVP_{347}$ are further normalized by their total 4MVP units, and the 4MVP-dependent harvesting efficiency of both (c) C.r. and (d) N.g. exhibits a fundamental transition between cationic NPPBs and linear-chain polymer flocculant P4MVP in dewatering microalgae.

become, and the smaller this number would be. The effect of the brush size diminishes when the brush gets longer.

Harvesting marine algae such as N.g. is notoriously difficult because of their small cell sizes, high oil contents, and the high density and salinity of the growth media.[15,42] It is surprising that cationic NPPBs directed similarly efficient dewatering (up to 100%) of both N.g. and C.r. following a similar dose-dependent behavior, although the slope of this dependency was less steep for each NPPB when it came to N.g (Figure 5b), likely because of the higher ionic strength of the growth media. In contrast, Fe_3O_4@SiO_2 and linear-chain $P4MVP_{347}$ only showed modest harvesting efficiency (<50%) for both algal species even at high doses. It is interesting to note that although NPPB−$P4MVP_{347}$ is a potent dewatering agent, the linear-chain $P4MVP_{347}$ brush by itself is powerless in dewatering N.g., agreeing with previous observations that polymer flocculants are inefficient on dewatering marine microalgae.[15,42] As for C.r., moderate dewatering efficiency (up to 50%) was reached for $P4MVP_{347}$ but only at a specific dosage. This also agrees with previous observations that careful choice of the dosages of polymer flocculants is important, as re-dissociation of the algae flocs occurs when the optimal dosage is surpassed.[39,40] Our zeta potential studies of the algae flocs helped clarify this delicate balance (Figure S6): initial adsorption of $P4MVP_{347}$ helps offset the anionic charges on algal cells, leading to increasing flocculation until the zeta potential approached zero. However, continuing adsorption of $P4MVP_{347}$ caused a charge inversion and re-dissociation of the algae flocs.

To gain further insight into the fundamental transition from chain-like polymer flocculants to NPPBs composed of the same polymer chains covalently grafted on a nanoparticle core, we normalized the dose-dependent harvesting efficiency of both algal species by the total number of cationic 4MVP units on individual NPPBs or $P4MVP_{347}$. We used the grafting densities determined by TGA to calculate the 4MVP unit concentrations, but the same behavior was observed when the grafting densities derived from the TEM analysis were used (not shown): a sharp transition from chain-like polymer flocculants to NPPBs in dewatering microalgae was clearly revealed (Figure 5c,d). In addition, an astonishing "master curve" showed up for all NPPBs, that is, regardless of the structural difference of the NPPBs, their harvesting efficiency appears to depend solely on, and increase almost linearly with, the total number of cationic 4MVP anchored to the anionic algal cells until nearly 100% of the cells is coagulated. This result highlights that Coulomb interaction is the major player regulating the colloidal stability of microalgae. The reason that higher dosages are needed for NPPBs of shorter brushes to reach a specific harvesting efficiency seems to be simply a numbers game, that is, to reach a threshold number of cationic units needed to offset the like-charge repulsions among a finite number of algal cells. The longer the brushes, the smaller the dosages needed to reach this number, and the less significant the dosage difference becomes. However, this simple picture cannot explain why the harvesting efficiency of linear-chain P4MVP remained low regardless of the dosages (Figure 5c,d). More insight into the underlying principles that govern the fundamental transition from chain-like polymer flocculants to NPPBs in dewatering microalgae entails computation and modeling, as will be discussed later.

Retrievable, Recyclable, and Reusable NPPBs. When flocculation is used to harvest microalgae, one outstanding challenge is the endless cost of flocculants and their potential contamination of downstream processes and the environment.[15−17] This deficiency is incompatible with large-scale algal biofuel productions. Although simpler methods that aim to reduce the attractive interactions between coagulated

DOI: 10.1021/acs.chemmater.9b00336
Chem. Mater. 2019, 31, 4657−4672

flocculants and microalgae have been reported, such as changing solution pH, organic solvent extraction, and/or increasing solution ionic strength,[73−77] the cost and efficiency of those methods need further scrutinization. In reality, once algal cells bind to flocculants, other forms of affinitive interactions such as van der Waals forces, coordination, physical entrapment, and so forth will all help maintain their close association. For instance, we tried to separate the NPPBs from algal cells by organic solvent extraction. Although the visually tempting biphasic solution seemed to suggest that algal cells were successfully separated from the cationic NPPBs, a closer look revealed that although algal oils and chromophores might enter the organic phase, other algal biomasses such as the cell wall components were still bound to the NPPBs (Figures S7 and 6e).

We reported previously that the ionic liquid [BMIM]Cl can dissolve chitosan for chemical modifications;[78] here, we show that it can also dissolve cellulose and other residual algal biomass after algal oil extraction. Optical microscopy pictures

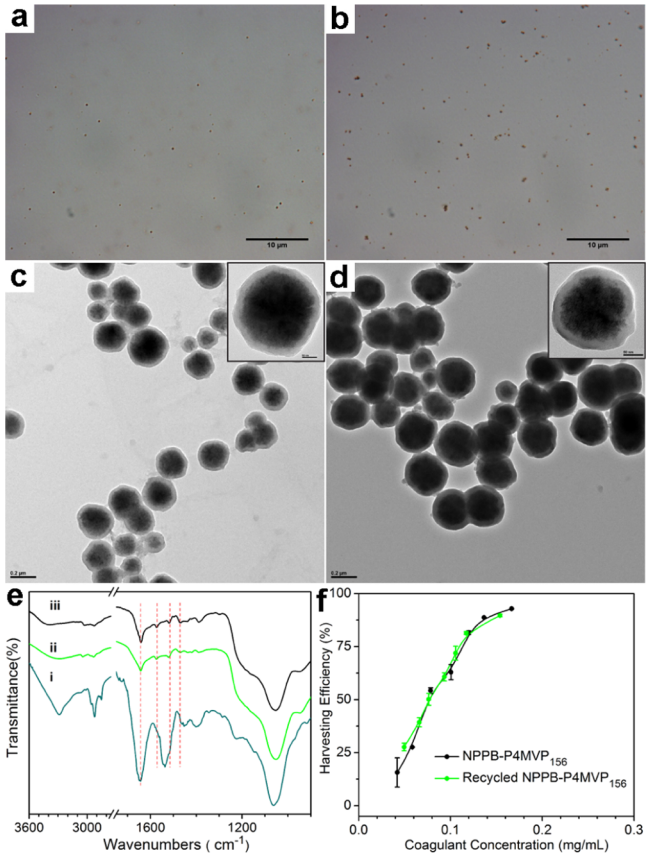

Figure 6. Retrievable, recyclable, and reusable NPPBs for microalgae harvesting. Optical microscopy reveals similarly well-dispersed cationic NPPBs (a) before microalgae dewatering and (b) after algal biomass removal by [BMIM]Cl (scale bar: 10 μm). TEM of NPPB−P4MVP$_{156}$ (c) before algae dewatering and (d) after biomass removal by [BMIM]Cl (scale bar: 0.2 μm) confirms that the "gray layer" (i.e., P4MVP$_{156}$ + SiO_2) thickness remains the same (inset: individual NPPB−P4MVP$_{156}$; scale bar: 50 nm). (e) FT-IR spectra of NPPB−P4MVP$_{156}$−algae biomass after (i) methanol/chloroform extraction, and (ii) [BMIM]Cl treatment compared to that of (iii) original NPPB−P4MVP$_{156}$. (f) Dose-dependent harvesting efficiency of C.r. by original (black trace) and recycled (green trace) NPPB−P4MVP$_{156}$.

of NPPB−P4MVP$_{156}$ before microalgae harvesting (Figure 6a) and after algal biomass removal by [BMIM]Cl (Figure 6b) revealed similarly well-dispersed NPPBs, in sharp contrast to those treated only by organic solvent extraction (Figure S7c). The hydrodynamic radius of recycled NPPB−P4MVP$_{156}$ was essentially the same as the original one with only a slight red shift of the peak position (~20 nm; Figure S8b). This slight difference could suggest the existence of NPPB-bound residue biomass or simply reflects a change of particle size distribution (i.e., the loss of smaller NPPBs) during the magnetophoretic separation of recycled NPPBs in the viscous ionic liquid media. Our additional analysis based on zeta potential, TEM, and FT-IR studies confirmed that the existence of NPPB-bound residue biomass was unlikely, and the structural integrity of NPPBs was fully recovered after the ionic liquid treatment. The zeta potential of recycled NPPB−P4MVP$_{156}$ was the same (58.60 ± 3.83 mV) as the original one (58.90 ± 1.89 mV), suggesting an unchanged P4MVP brush structure (Figure S8a). Under TEM, the P4MVP brushes carry high-electron-density iodide counterions, hence displaying little contrast to the silica layer of NPPBs. Quantitative analysis of the entire "gray layer" thickness (i.e., SiO_2 + P4MVP$_{156}$) of individual NPPB−P4MVP$_{156}$ before microalgae harvesting (Figure 6c; 32.4 ± 6.7 nm) and after algal biomass removal by [BMIM]Cl (Figure 6d; 32.4 ± 8.6 nm) showed essentially no difference, suggesting the structural integrity of NPPBs survived the ionic liquid treatment. The FT-IR spectrum of the coagulated C.r. and NPPB−P4MVP$_{156}$ biomass after algal oil extraction by organic solvents (Figure 6e, trace i) showed strong absorption around 2920, 1633, 1515, 1449, and 1024 cm^{-1}, which are characteristic peaks of the residual algal biomass (Figure S9). After [BMIM]Cl treatment (trace ii), all algal absorption peaks were gone and the FT-IR spectrum was almost identical to that of the original NPPB−P4MVP$_{156}$ (trace iii), with the four fingerprint pyridinium frequencies clearly revealed (marked by red dotted lines). The recycled NPPB−P4MVP$_{156}$ was retrieved by a magnet and directly reused for repeated microalgae harvesting with uncompromised dewatering efficiency (Figure 6f): the dose-dependent harvesting efficiency of C.r. by recycled NPPB−P4MVP$_{156}$ (green trace) overlapped nicely with that of the original NPPB (black trace), reaching 90% for both NPPBs at a similar dose (~0.16 mg/mL) that we tested.

Covalent grafting of polymer brushes onto the solid-state, paramagnetic nanoparticles enables facile retrieval and recycle of the entire NPPBs to be directly reused for successive dewatering. The importance of this aspect cannot be overstated because it greatly reduces the endless material cost on flocculants and their potential contamination of downstream processes and the environment. Unlike previous reports on recyclable coagulation agents that involve complex regeneration processes, such as magnetite nanoparticles that were released from algal biomass by dissolution in strong acids and resynthesized;[21] or charge-reversal polymer flocculants that were released from algal biomass by changing solution pH, separated out by centrifugation to remove algal biomass, and recovered by lyophilization;[46] or nanoparticles coated with UV-oxidizable steric acids that were released from algal biomass by UV irradiation and possibly regenerated by separating out the nanoparticles and recoating them with steric acids;[79] our design differs in that we adapt an ionic-liquid-based green chemistry approach[78,80,81] to remove the residual algal biomass after algal oil extraction and a facile

DOI: 10.1021/acs.chemmater.9b00336
Chem. Mater. 2019, 31, 4657−4672

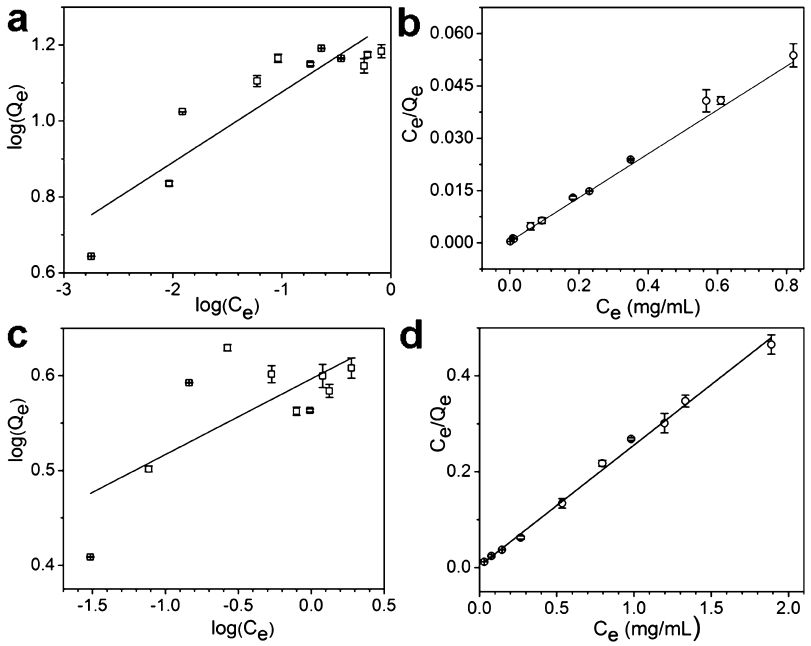

Figure 7. Adsorption isotherms between microalgae and cationic NPPBs. The adsorption data of C.r. (a,b) and N.g. (c,d) are fit with the Freundlich (a,c) and Langmuir (b,d) isotherm models, respectively, as shown in the solid lines.

magnetophoretic separation process to retrieve the NPPBs that are directly reusable for additional rounds of operations. Our design also differs from the combinatorial approaches that either mixed polymer flocculants with microalgae before adding magnetite particles or mixed polymer flocculants with magnetite particles before adding microalgae.[72,82,83] In those approaches, the cationic polymers acted as binders to bring the otherwise repulsive magnetite particles and algal cells together, which improved the harvesting efficiency of both flocculants when they are used alone.[72] However, it is a challenge in those approaches to separate either the polymers or magnetite particles from algal biomass, let alone recycle and reuse them. In our design, the polymer brushes are covalently grown on and stay with the nanoparticles, allowing the entire NPPBs to be retrieved and recycled for repeated rounds of microalgae dewatering.

It is worth noting that the same [BMIM]Cl treatment worked equally well on recycling bare nanoparticles (i.e., Fe_3O_4 and Fe_3O_4@SiO_2) that do not have the covalently grafted polymer brushes (Figure S10). We expect that the use of ionic liquids for algal biomass removal has broad utility to retrieve, recycle, and reuse solid-state coagulants. Ionic liquids are considered as "green" solvents because their high boiling point and low volatility not only help minimize their undesired release into environment during the operations but also allow them to be easily recycled and reused afterward (e.g., biomass in ionic liquids can be precipitated out by other solvents, and those solvents can be further recovered by distillation). The retrieve, recycle, and reuse of NPPBs showed no adverse effects on continuous algaculture (Figure S11); this is another great advantage when water itself is a precious resource (e.g., algaculture in desert land). We are cautiously optimistic that the development of NPPBs for microalgae dewatering and ionic liquids to recycle and reuse the NPPBs may help pave the way for cost-effective algal biofuel production at large scales.

Mechanistic Insight of the NPPB–Algae Interactions. The adsorption isotherms between microalgae and cationic NPPBs clearly fit the Langmuir rather than the Freundlich model (Figure 7), suggesting that the NPPBs only interact with one layer of algal cells, that is, the polymer brushes on NPPBs do not extend their actions beyond their closest neighbors of algal cells. In addition, the Langmuir isotherm also indicates the lack of incongruous interactions between NPPBs and algal cells that would otherwise induce the coagulation of algal cells beyond their closest neighbors (e.g., due to the released extracellular substances), or the physical entrapment of additional algal cells that do not interact with NPPBs directly. Similar adsorption isotherms were observed previously between algae and bare Fe_3O_4 nanoparticles with[84] and without[21,24] the presence of free polymer flocculants, although Freundlich-type isotherms were also observed in the former case.[85] The maximum adsorption capacity (Q_m) for C.r. was 15.90 ± 0.12 per unit mass of NPPB–$P4MVP_{245}$, and that for N.g. was 4.01 ± 0.09 per unit mass of NPPB–$P4MVP_{198}$, with R^2 = 0.99 in both fittings. The Langmuir constant (K_L), which describes the stability of adsorption, was 163.41 ± 29.66 and 79.58 ± 21.27 mL/mg for C.r. and N.g., respectively. This number is 1–2 orders of magnitude higher than that observed between bare Fe_3O_4 nanoparticles and microalgae,[21,24] suggesting more favorable interactions between cationic NPPBs and algal cells.

To better understand and potentially optimize the design of NPPBs for microalgae dewatering, we used computation and modeling to correlate the structural characteristics of NPPBs with the resultant microalgae dewatering efficiency. The NPPBs with well-defined polymer brushes serve nicely as model systems to test the underlying principles governing the phase separation of solution–borne planktonic cells. Details of our method are discussed in the Supporting Information. In brief, we adapted the classic DLVO theory[49] as the starting point to model the colloidal stability of algal cells in the presence of cationic NPPBs. Although the surface of typical live cells is fuzzy, heterogeneous, and undergoes dynamic changes, we treated algal cells as smooth spheres (with radius

DOI: 10.1021/acs.chemmater.9b00336
Chem. Mater. 2019, 31, 4657–4672

Table 2. Experimental and Theoretical Properties of Model NPPBs

cationic NPPBs	L_b (nm)[a]	L_b^* (nm)[b]	D_{min} (nm)[c]	$F_{NPPB-algae}$ (kT/nm^2)[d]	k_c	k^*
Fe_3O_4@SiO_2@P4MVP$_{67}$	45.4	44.1	24.5	−379.6	887	1119
Fe_3O_4@SiO_2@P4MVP$_{156}$	96.0	97.3	63.0	−534.7	77	648
Fe_3O_4@SiO_2@P4MVP$_{198}$	123.5	130.9	87.5	−565.3	12	489
Fe_3O_4@SiO_2@P4MVP$_{245}$	151.2	161.7	112.0	−585.7	2	389
Fe_3O_4@SiO_2@P4MVP$_{347}$	204.4	231.0	168.0	−612.2	1	252

[a]Brush lengths of free cationic NPPBs in solution measured by DLS. [b]Theoretical values computed from SCFT: Brush lengths of free cationic NPPBs in solution. [c]Theoretical values computed from SCFT: Cationic NPPB-algae separations at equilibrium. [d]Theoretical values computed from SCFT: Cationic NPPB-algae interaction free energy at equilibrium.

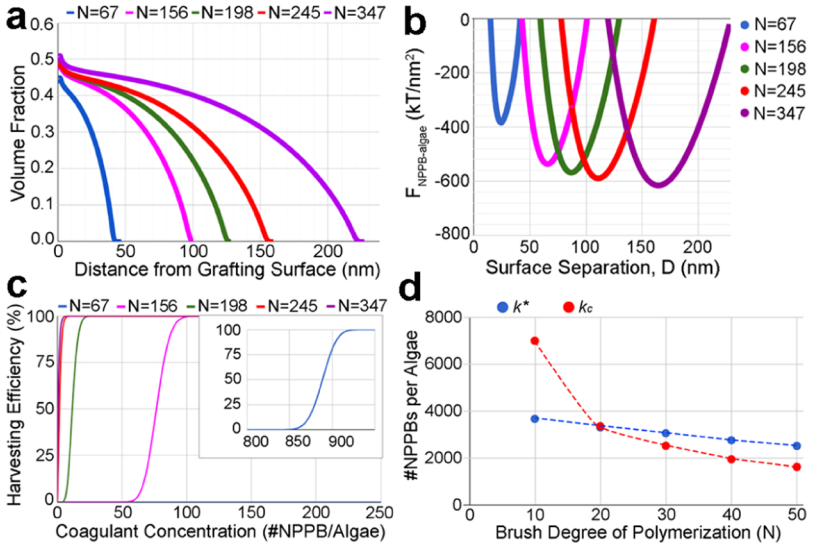

Figure 8. Computations based on DLVO theory and SCFT analysis reveal mechanistic insight on NPPB-directed microalgae dewatering. (a) Brush profiles of cationic NPPBs in water. (b) NPPB−algae pair-potentials vary with the brush sizes N (i.e., DP) and the surface separation, D, between the Fe_3O_4@SiO_2 and algal cell. The huge and increasing energy wells that show up as brushes get longer indicate the balance of enthalpy gains from Coulombic attractions and entropy costs from spring-like resistance of the brushes upon deformation. (c) Simulated harvesting efficiency of NPPBs (inset: NPPB−P4MVP$_{67}$). (d) Comparison of k_c and k^* as a function of brush size reveals a minimum size requirement (i.e., DP ≥ 20 for the current configuration) to satisfy $k_c \leq k^*$, a prerequisite for dewatering algae.

r = 4 μm) with a uniform and constant charge density on the length scale of the NPPBs and time scale of the dewatering tests. The response of the polymer brushes in a solution of ions, NPPBs, and algal cells was modeled by the self-consistent field theory (SCFT).[86−89] Unlike DLVO, SCFT allows modeling multicomponent effects on the conformational changes of the polymer brushes, hence providing much greater structural information on the NPPB−microalgae interactions. It also allows the determination of the interaction free energy $F(D)$ as a function of the separation distance D between the surface of an algae cell and the grafting surface of NPPBs. Our method differs from the extended DLVO model (XDLVO) adapted by others, in which electron donor−acceptor interactions were added to introduce attractions between magnetic particles and algal cells that are otherwise missing in classic DLVO theory.[77,83,90] Not only will this approach require meaningful contact angle measurement of both algae and NPPBs to derive their surface tension components if used in our system, but also it will neglect the dynamic nature of polymer chains, their responses to solution properties, their quantitative aspects such as sizes, charge density, and surface number density, entropic contributions, and so forth. In contrast, SCFT uses a mean field approach to account for all of the above factors while including multicomponent interactions. The thermodynamic properties of the system are obtained through convergence of a self-consistent calculation.

Experimentally, harvesting efficiency was determined as the percentage of algal cells removed from an algae culture. A cell is removed if: (i) it forms a cluster with cationic NPPBs and other algal cells, and (ii) the number of cationic NPPBs in that cluster is large enough such that the magnetophoretic force overcomes random Brownian motions. Here, we assume that the number of cationic NPPBs required to form any cluster of algae is sufficiently large to respond to the magnet. Thus, the harvesting efficiency is assumed to be solely dependent on the ability of the algal cells to form clusters. SCFT computation (Table 2) shows that once a cationic NPPB comes in close contact with an algal cell, an irreversible association toward the minimum potential well of $F(D)$ occurs with a huge gain of free energy ($F \approx -10^2$ to 10^3 kT/nm^2). The force between any NPPB-coated algal cells becomes the sum of algae−algae, NPPB−NPPB, and algae−NPPB interaction forces, each of which can be determined analytically (i.e., $-\partial F/\partial D$). Clusters will form when the sum of all forces is attractive (negative).

We treated the cationic NPPBs as "Debye balls", that is, spheres with radii equivalent to the summation of the Fe_3O_4@SiO_2 radius (~100 nm), the P4MVP brush length (Table 2), and the Debye length. Each algal cell provides only a finite number k^* of NPPB binding sites on its surface, equal to the

DOI: 10.1021/acs.chemmater.9b00336
Chem. Mater. 2019, 31, 4657−4672

contact surface area divided by the projected area of a Debye ball. For a specific Debye ball, there is also a threshold NPPB-per-algae number, k_c, beyond which the NPPB−algae attractions will overcome the algae−algae and NPPB−NPPB repulsions. Microalgae are only harvested when the actual NPPB-per-algae number, k, satisfies $k_c \leq k \leq k^*$. If the number of algae in our system defined as A, we can add n NPPBs that irreversibly attach to algae cells. What then is the probability (i.e., harvesting efficiency) that a given algal cell has k equal to or greater than k_c of its available k^* sites occupied by NPPBs? This problem can be described by the hypergeometric probability distribution.

It may help to draw parallels to a more traditional example of the hypergeometric distribution. Imagine a population of $N = Ak^*$ marbles, where there are A different colors and k^* of each color. We then grab a handful of n marbles and count how many marbles of each color we have. By analogy, say we have $A = 3$ algal cells in an algae culture, where each cell has $k^* = 4$ binding sites. Therefore, we have $N = 12$ total marbles. The color is arbitrary, but we will say there are 4 red, 4 blue, and 4 white, with each color representing an algal cell. Reaching into the bag of marbles to pick 3 is analogous to dropping 3 cationic NPPBs into the algae culture. We could have picked 1 white, 1 blue, and 1 red, or 2 white, 1 blue, and no red, so on and so forth. Picking 2 whites, 1 blue, and no red means that the NPPBs are attached to 2 sites on one algal cell, 1 site on another, and none on the third. Depending on the k_c and k^* values of different NPPBs, we will then be able to calculate the probability of a given algal cell that has at least k_c of its k^* available sites occupied by NPPBs.

Experimental and theoretical properties of model NPPBs are compared in Table 2, with a few example simulations graphed in Figure 8. Given that the Debye length of algae solutions can range from ∼1000 nm (i.e., pure fresh water) to 1 nm (i.e., brine water with an ionic strength of ∼100 mM), we used an example Debye length of 25 nm, a P4MVP grafting density of 0.61 chains/nm^2, and an algae charge density of 70 e/nm^2 in the computations. The P4MVP grafting density was chosen based on experimental values (Table 1). The algae charge density was measured during dewatering tests (Figure S16) and is in line with reported values (∼10−200 e/nm^2) of various algal species at different pHs.[91] The brush lengths of cationic NPPBs in the solution were determined by DLS as the difference in hydrodynamic radii between the cationic NPPBs and Fe_3O_4@SiO_2 (Figure S12) and agree well with computed values from SCFT (Table 2, Figure 8a).

The pair potentials between NPPB-coated algal cells were taken to be a sum of algae−algae, NPPB−NPPB, and algae−NPPB interactions and computed individually to obtain interaction forces. As an example, the NPPB−algae pair potentials as a function of Fe_3O_4@SiO_2 and algal cell surface separation are shown (Figure 8b). The irreversible binding between the two is evident as the deep energy wells at the equilibrium separations, reflecting a delicate balance between enthalpy gains from Coulomb attractions of the oppositely charged surfaces and entropy costs from spring-like resistance when the brushes are constricted upon interacting with an algal cell.

The NPPBs bound to one algal cell can use their free-polymer brushes to bridge another algal cell as long as the sum of all interaction forces is attractive and the required number of NPPBs on the algal cell is physically possible (i.e., $k_c \leq k^*$). The theoretical dose-dependent algal harvesting efficiency of cationic NPPBs agrees well with experiments (Figure 8c): a lower dose is needed for NPPBs of longer brushes to reach the same harvesting efficiency, but the benefit of longer brushes diminishes with increasing brush lengths. This "level-off" behavior is more than a simple numbers game of charge matching as we speculated earlier (Figure 5). Rather, it results from the synergistic actions of two opposite interaction forces: the first is the algae−algae and NPPB−NPPB electrostatic double-layer repulsions that decay exponentially as the separation between the algal cells increases. As clearly shown in Table 2, the threshold k_c needed to overcome interalgae repulsions decreases rapidly as the brush length (i.e., interalgae separation or NPPB size) increases, which naturally levels out as k_c eventually reaches 1; the second is the NPPB−algae Coulombic attraction that increases as the brushes get longer (Figure 8b), which also leads to smaller k_c and can be understood by considering each brush as the same type of spring composed of the same P4MVP backbone. The longer the spring, the "softer" it becomes, and the less entropy cost it has to endure to gain attractive Coulombic interactions by constricting itself against the oppositely charged algal cell. This increasing coulombic attraction also levels out, again because the decreasing k_c eventually reaches 1.

Although NPPBs do not have to carry long brushes to become supercoagulants, they do need a minimum brush size to disrupt the colloidal stability of algal cultures. With the current simulation configuration, our model predicts a minimum brush DP of ∼20 (Figure 8d), below which the number of NPPBs per algae needed to overcome interalgae repulsions is more than the maximum available binding sites on the algae (i.e., $k_c > k^*$). It is the existence of this minimum brush DP rather than its value per se that is important, as the computed value depends on modeling parameters. Although it is experimentally difficult to prepare well-defined but extremely short polymer brushes via SI-ATRP to test this prediction, we did observe the deterioration of cationic NPPBs in harvesting microalgae when their brush length is shortened (Figure 5). Because our computations neglected the effect of magnetic field, this minimum brush length prediction simply highlights what it takes for a given NPPB configuration to flocculate algae. In practice, even bare paramagnetic particles without polymer brushes (i.e., DP = 0) were tested for algae dewatering.[20−24] Our model and own experiments (Figures 5 and S10) suggest that in those tests, the dewatering efficiency relies on magnetophoretic forces and has little to do with flocculation.

It is worthwhile to ponder the implications of our computations and the design concepts of NPPBs. First, why are the cationic NPPBs supercoagulants while the chain-like brushes by themselves lag far behind in effectiveness? The fundamental difference lies in their different modes of interaction with algal cells (Figure 9). The chain-like polymer flocculants, regardless of their sizes and microstructures (e.g., branching), inevitably condense on the oppositely charged algal cells with a high surface coverage to maximize their coulombic attractions. This process is counteracted by the entropy cost, repulsion between repeating units, and polymer−solution interactions that all contribute to the formation of suspending chain loops or dangling chain ends,[39,40,53,54] but these segments are often too short to reach neighboring algal cells kept apart by their like-charge repulsions (Figure 9a). As we demonstrated unambiguously (Figures 5 and S6), chain-like polymer flocculants work at their best at the critical surface

DOI: 10.1021/acs.chemmater.9b00336
Chem. Mater. 2019, 31, 4657−4672

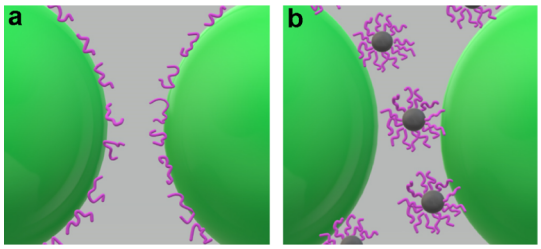

Figure 9. Fundamental difference between cationic NPPBs and polymer flocculants in dewatering microalgae. (a) Polymer flocculants are adsorbed on the algal cell surface at multiple sites along their chains, such that their chain loops or dangling chain ends are often too short to bridge neighboring algal cells kept apart by like-charge repulsions. (b) NPPBs with covalently grafted polymer chains are transformed into super-coagulants because the solid-state core and extended brush conformation help NPPBs reach out to neighboring algal cells and overcome their like-charge repulsions to form clusters.

coverage that offsets all of the charges on algal cells. This is a delicate charge matching—both under and overdosing shift the balance in favor of like-charge repulsions. In contrast, the cationic NPPBs are designed to mimic bacterial outer membrane vesicles that help bridge planktonic bacteria to form biofilms,[55,56] and they "extend out" rather than "lie down" on algal cell surfaces. The spring-like entropic resistance quickly overturns any free-energy gain from Coulomb attractions if their brushes are constricted against algal cells (Figure 8b). Together with an incompressible solid-state core, NPPBs reach out to neighboring algal cells at a greater distance where the interalgae like-charge repulsions are feeble and can be easily overcome (Figure 9b, also see Figure 4f).

Second, how can we optimize the design of NPPBs for microalgae dewatering, or more generally for the selective capture and separation of solution–borne live cells? The key concept is to provide a guaranteed spacing between neighboring cells such that the intercell repulsions are no match for the attractive bridging forces. This can be achieved with a bigger NPPBs with either a larger solid-state core or longer polymer brushes, or both. The trade-off, however, is to maintain $k_c \leq k^*$ as both options decrease k^*. The typical cell sizes in micrometer-ranges sets the maximum size limit of the core (i.e., $k^* \rightarrow 1$), beyond which the mode of action changes from coagulation to surface adsorption as gravity will make it difficult for the particles to be dispersed in the solution and freely interact with live cells. In the other direction, the particle core can be made very small in theory as long as the overall sizes of NPPBs are compensated by very long polymer brushes, although this is experimentally challenging in practice. We contemplate that our current design of the solid-state core with a size in the 100 nm-range is a good compromise. As for the length of the brushes, our model predicts a minimum brush size requirement for a given NPPB-cell system. The longer the brushes, the more powerful their bridging interactions but the more difficult their synthesis. Fortunately, the benefit of increasing brush size quickly wanes as brushes get longer. In our system, the power of cationic NPPBs on dewatering microalgae plateaus at an optimal brush DP $\approx$ 200 (Figure 5c,d), which is readily reachable via SI-ATRP.

Finally, we should point out the limitations of our computations. Because of the difficulty of incorporating steric repulsions, our DLVO model only considers van der Waals and electrical double-layer interactions by assuming a smooth algal cell surface. This assumption will likely fall as the Debye length becomes smaller than the working distance of steric repulsions. Additionally, our model assumes perfect mixing during dewatering tests, that is, each algal cell is able to grab any available NPPBs freely. This assumption is acceptable for the small test volume we use but may need to be revisited for large-scale operations. Nevertheless, our theoretical framework captures the basic behavior of NPPB-directed spontaneous microalgae dewatering. It agrees well with experimental data and provides insights on the design concepts of NPPBs that could be further adapted to harvest solution–borne live cells in general.

CONCLUSIONS

In summary, we report here a conceptual design of retrievable, recyclable, and reusable NPPBs as supercoagulants for microalgae dewatering. The colloidal stability of planktonic cells hinges on the different working distances of counteracting forces. The attractive forces (such as the van der Waals force) usually decay with separation quicker than the repulsive ones (such as the like-charge repulsion),[49] such that auto-flocculation is prohibited. A key strategy to break this balance is to introduce attractive forces over longer distances. Compared to many other reports on harvesting microalgae, we took an inspiration from biology by mimicking bacterial outer membrane vesicles in promoting coaggregation of planktonic bacteria toward biofilm formation and focused our design on the retrievability, recyclability, and reusability of the coagulation agents. This "R3" criterion, in our opinion, is the cornerstone of a sustainable algae-based biofuel economy because it is the ultimate requirement to reduce energy cost, material cost, and environmental footprint for large-scale operations.

In the pursuit of coagulation agents to break the technology bottleneck forestalling the commercialization of algal biofuels, much attention has been put on comparing the harvesting efficiency of different approaches. Such comparison without context offers little value because it not only neglects the big picture of sustainability but also overlooks the fact that harvesting efficiency itself depends on many experimental variables, including the doses of coagulation agents, algae concentrations, interaction times, solution properties, and so forth. There is an imperative need to standardize dewatering protocols such that meaningful comparison between different designs can be made. Our exploratory effort on standardized dewatering tests clearly displays the difference between cationic NPPBs and two other frequently used coagulation agents, that is, inorganic particles and polymer flocculants. Using NPPBs with well-defined polymer brushes as models and a two-pronged approach that integrates experiments with computations, we elucidated the fundamental transition from chain-like polymer flocculants to NPPBs and the design concepts of NPPBs for microalgae dewatering. Because the structurally versatile polymer brushes on the NPPBs can be designed to introduce various types of attractive forces besides the charge interaction, such as H-bonding, ionic bridging, chemical coordination, and so forth, the concepts learnt here will not only help free the great potential of algal biofuels but also may benefit other fields where selective capture and separation of solution–borne planktonic cells is a challenging task, or applications involving rational control of colloidal stability (e.g., advanced inks, photonic crystals, etc.).

DOI: 10.1021/acs.chemmater.9b00336
Chem. Mater. 2019, 31, 4657–4672

■ ASSOCIATED CONTENT

Supporting Information

The Supporting Information is available free of charge on the ACS Publications website at DOI: 10.1021/acs.chemmater.9b00336.

Synthesis of NPPBs and additional experimental data and computation approaches to understand NPPB-directed spontaneous microalgae dewatering (PDF)

In sharp contrast to polymer flocculants or bare magnetic nanoparticles, adding cationic NPPBs into algae cultures triggered rapid phase separation of the solution into coagulated algal biomass and supernatant (AVI)

■ AUTHOR INFORMATION

Corresponding Author

*E-mail: H.Liang@ttuhsc.edu.

ORCID

Wan Zheng: 0000-0002-5475-5340

Hongjun Liang: 0000-0003-0864-9106

Present Address

#Schepens Eye Research Institute of Massachusetts Eye and Ear, Harvard Medical School, Boston, MA 02114.

Notes

The authors declare the following competing financial interest(s): A patent was issued on the conceptual design of NPPBs for harvesting microalgae (#US 9,464,268 B2).

■ ACKNOWLEDGMENTS

We are grateful for financial supports from NSF CBET 1623240 and 1160291, COEDIT #12B GF-72, and a seed grant from C2B2. We thank Drs. Daoben Hua, Huiya Gu, Robert Jinkerson, and Randor Radakovits for their help. J.G. and L.K. acknowledge graduate fellowships received from the US Air Force and C2B2-Chevron, respectively.

■ ABBREVIATIONS

NPPB, nanoparticle-pinched polymer brushes; P4VP, poly(4-vinylpyridine); P4MVP, poly(4-vinyl-*N*-methylpyridine iodide); DP, degree of polymerization; PDI, polydispersity index; C.r., *Chlamydomonas reinhardtii*; N.g., *Nannochloropsis gaditana*; DCW, dry cell weight; OD, optical density; SI-ATRP, surface-initiated atom transfer radical polymerization; SCFT, self-consistent field theory; TEM, transmission electron microscope; GPC, gel permeation chromatography; FT-IR, Fourier transform infrared spectroscopy; TGA, thermal gravimetric analysis; DLS, dynamic light scattering

■ REFERENCES

(1) Fossil Fuels; The National Academy of Sciences. http://needtoknow.nas.edu/energy/energy-sources/fossil-fuels/ (accessed April 5, 2018).

(2) Use of Energy in the United States; U.S. Energy Information Administration. https://www.eia.gov/energyexplained/?page=us_energy_transportation (accessed April 5, 2018).

(3) Hess, J.; Bednarz, D.; Bae, J.; Pierce, J. Petroleum and Health Care: Evaluating and Managing Health Care's Vulnerability to Petroleum Supply Shifts. *Am. J. Public Health* **2011**, *101*, 1568−1579.

(4) Chisti, Y. Biodiesel from Microalgae. *Biotechnol. Adv.* **2007**, *25*, 294−306.

(5) Wijffels, R. H.; Barbosa, M. J. An Outlook on Microalgal Biofuels. *Science* **2010**, *329*, 796−799.

(6) Mata, T. M.; Martins, A. A.; Caetano, N. S. Microalgae for Biodiesel Production and Other Applications: A Review. *Renewable Sustainable Energy Rev.* **2010**, *14*, 217−232.

(7) Greenwell, H. C.; Laurens, L. M. L.; Shields, R. J.; Lovitt, R. W.; Flynn, K. J. Placing Microalgae on the Biofuels Priority List: A Review of the Technological Challenges. *J. R. Soc., Interface* **2010**, *7*, 703−726.

(8) Sheehan, J.; Dunahay, T.; Benemann, J.; Roessler, P. G. *A Look Back at the US Department of Energy's Aquatic Species Program—Biodiesel from Algae*, Close-Out Report TP-580-2419; US Department of Energy's Office of Fuels Development, 1998, available at http://www.nrel.gov/docs/legosti/fy98/24190.pdf.

(9) Dismukes, G. C.; Carrieri, D.; Bennette, N.; Ananyev, G. M.; Posewitz, M. C. Aquatic Phototrophs: Efficient Alternatives to Land-Based Crops for Biofuels. *Curr. Opin. Biotechnol.* **2008**, *19*, 235−240.

(10) Hu, Q.; Sommerfeld, M.; Jarvis, E.; Ghirardi, M.; Posewitz, M.; Seibert, M.; Darzins, A. Microalgal Triacylglycerols as Feedstocks for Biofuel Production: Perspectives and Advances. *Plant J.* **2008**, *54*, 621−639.

(11) Shen, Y.; Yuan, W.; Pei, Z. J.; Wu, Q.; Mao, E. Microalgae Mass Production Methods. *Trans. ASABE* **2009**, *52*, 1275−1287.

(12) Gerardo, M. L.; Van Den Hende, S.; Vervaeren, H.; Coward, T.; Skill, S. C. Harvesting of Microalgae within a Biorefinery Approach: A Review of the Developments and Case Studies from Pilot-Plants. *Algal Res.* **2015**, *11*, 248−262.

(13) Baicha, Z.; Salar-García, M. J.; Ortiz-Martínez, V. M.; Hernández-Fernández, F. J.; de los Ríos, A. P.; Labjar, N.; Lotfi, E.; Elmahi, M. A Critical Review on Microalgae as an Alternative Source for Bioenergy Production: A Promising Low Cost Substrate for Microbial Fuel Cells. *Fuel Process. Technol.* **2016**, *154*, 104−116.

(14) Zhu, L.; Nugroho, Y. K.; Shakeel, S. R.; Li, Z.; Martinkauppi, B.; Hiltunen, E. Using Microalgae to Produce Liquid Transportation Biodiesel: What Is Next? *Renewable Sustainable Energy Rev.* **2017**, *78*, 391−400.

(15) Uduman, N.; Qi, Y.; Danquah, M. K.; Forde, G. M.; Hoadley, A. Dewatering of Microalgal Cultures: A Major Bottleneck to Algae-Based Fuels. *J. Renewable Sustainable Energy* **2010**, *2*, 012701.

(16) Milledge, J. J.; Heaven, S. A Review of the Harvesting of Micro-Algae for Biofuel Production. *Rev. Environ. Sci. Bio/Technol.* **2013**, *12*, 165−178.

(17) Barros, A. I.; Gonçalves, A. L.; Simões, M.; Pires, J. C. M. Harvesting Techniques Applied to Microalgae: A Review. *Renewable Sustainable Energy Rev.* **2015**, *41*, 1489−1500.

(18) Bosma, R.; van Spronsen, W. A.; Tramper, J.; Wijffels, R. H. Ultrasound, A New Separation Technique to Harvest Microalgae. *J. Appl. Phycol.* **2003**, *15*, 143−153.

(19) Gómez, E. H.; Tryner, J.; Aligata, A. J.; Quinn, J. C.; Marchese, A. J. Measurement of Acoustic Properties of Microalgae and Implications for the Performance of Ultrasonic Harvesting Systems. *Algal Res.* **2018**, *31*, 77−86.

(20) Bitton, G.; Fox, J. L.; Strickland, H. G. Removal of Algae from Florida Lakes by Magnetic Filtration. *Appl. Microbiol.* **1975**, *30*, 905−908.

(21) Xu, L.; Guo, C.; Wang, F.; Zheng, S.; Liu, C.-Z. A Simple and Rapid Harvesting Method for Microalgae by in situ Magnetic Separation. *Bioresour. Technol.* **2011**, *102*, 10047−10051.

(22) Cerff, M.; Morweiser, M.; Dillschneider, R.; Michel, A.; Menzel, K.; Posten, C. Harvesting Fresh Water and Marine Algae by Magnetic Separation: Screening of Separation Parametersand High Gradient Magnetic Filtration. *Bioresour. Technol.* **2012**, *118*, 289−295.

(23) Wang, S.-K.; Stiles, A. R.; Guo, C.; Liu, C.-Z. Harvesting Microalgae by Magnetic Separation: A Review. *Algal Res.* **2015**, *9*, 178−185.

(24) Hu, Y.-R.; Wang, F.; Wang, S.-K.; Liu, C.-Z.; Guo, C. Efficient Harvesting of Marine Microalgae Nannochloropsis maritima Using Magnetic Nanoparticles. *Bioresour. Technol.* **2013**, *138*, 387−390.

(25) Stephens, E.; Ross, I. L.; King, Z.; Mussgnug, J. H.; Kruse, O.; Posten, C.; Borowitzka, M. A.; Hankamer, B. An Economic and Technical Evaluation of Microalgal Biofuels. *Nat. Biotechnol.* **2010**, *28*, 126−128.

DOI: 10.1021/acs.chemmater.9b00336
Chem. Mater. 2019, 31, 4657−4672

(26) Chen, C.-Y.; Yeh, K.-L.; Aisyah, R.; Lee, D.-J.; Chang, J.-S. Cultivation, Photobioreactor Design and Harvesting of Microalgae for Biodiesel Production: A Critical Review. *Bioresour. Technol.* **2011**, *102*, 71−81.
(27) Christenson, L.; Sims, R. Production and Harvesting of Microalgae for Wastewater Treatment, Biofuels, and Bioproducts. *Biotechnol. Adv.* **2011**, *29*, 686−702.
(28) Pragya, N.; Pandey, K. K.; Sahoo, P. K. A Review on Harvesting, Oil Extraction and Biofuels Production Technologies from Microalgae. *Renewable Sustainable Energy Rev.* **2013**, *24*, 159−171.
(29) Proctor, C. R.; Hammes, F. Drinking Water Microbiology - From Measurement to Management. *Curr. Opin. Biotechnol.* **2015**, *33*, 87−94.
(30) O'Toole, G.; Kaplan, H. B.; Kolter, R. Biofilm Formation as Microbial Development. *Annu. Rev. Microbiol.* **2000**, *54*, 49−79.
(31) Qian, W.; Zhang, Y.; Chen, W. Capturing Cancer: Emerging Microfluidic Technologies for the Capture and Characterization of Circulating Tumor Cells. *Small* **2015**, *11*, 3850−3872.
(32) Grima, E. M.; Belarbi, E. H.; Fernandez, F. G. A.; Medina, A. R.; Chisti, Y. Recovery of Microalgal Biomass and Metabolites: Process Options and Economics. *Biotechnol. Adv.* **2003**, *20*, 491−515.
(33) Patil, V.; Tran, K.-Q.; Giselrød, H. R. Towards Sustainable Production of Biofuels from Microalgae. *Int. J. Mol. Sci.* **2008**, *9*, 1188−1195.
(34) Pienkos, P. T.; Darzins, A. The Promise and Challenges of Microalgal-Derived Biofuels. *Biofuels, Bioprod. Biorefin.* **2009**, *3*, 431−440.
(35) Chen, Y. M.; Liu, J. C.; Ju, Y.-H. Flotation Removal of Algae from Water. *Colloids Surf., B* **1998**, *12*, 49−55.
(36) Liu, J. C.; Chen, Y. M.; Ju, Y.-H. Separation of Algal Cells from Water by Column Flotation. *Sep. Sci. Technol.* **1999**, *34*, 2259−2272.
(37) Phoochinda, W.; White, D. A.; Briscoe, B. J. An Algal Removal Using a Combination of Flocculation and Flotation Processes. *Environ. Technol.* **2004**, *25*, 1385−1395.
(38) Chen, J. J.; Yeh, H. H.; Tseng, I. C. Potassium Permanganate as an Alternative Preoxidant for Enhancing Algal Coagulation - Pilot and Bench Scale Studies. *Environ. Technol.* **2008**, *29*, 721−729.
(39) Tenney, M. W.; Echelberger, W. F.; Schuessler, R. G.; Pavoni, J. L. Algal Flocculation with Synthetic Organic Polyelectrolytes. *Appl. Microbiol.* **1969**, *18*, 965−971.
(40) Tilton, R. C.; Murphy, J.; Dixon, J. K. Flocculation of Algae with Synthetic Polymeric Flocculants. *Water Res.* **1972**, *6*, 155−164.
(41) Shelef, G. A.; Sukenik, A.; Green, M. *Microalgae Harvesting and Processing: A Literature Review*, report: SERI/STR-231-2396, 1984, available at http://www.nrel.gov/docs/legosti/old/2396.pdf.
(42) Bilanovic, D.; Shelef, G.; Sukenik, A. Flocculation of Microalgae with Cationic Polymers - Effects of Medium Salinity. *Biomass* **1988**, *17*, 65−76.
(43) Divakaran, R.; Sivasankara Pillai, V. N. Flocculation of Algae Using Chitosan. *J. Appl. Phycol.* **2002**, *14*, 419−422.
(44) Knuckey, R. M.; Brown, M. R.; Robert, R.; Frampton, D. M. F. Production of Microalgal Concentrates by Flocculation and Their Assessment as Aquaculture Feeds. *Aquacult. Eng.* **2006**, *35*, 300−313.
(45) Vandamme, D.; Foubert, I.; Muylaert, K. Flocculation as a Low-Cost Method for Harvesting Microalgae for Bulk Biomass Production. *Trends Biotechnol.* **2013**, *31*, 233−239.
(46) Morrissey, K. L.; He, C.; Wong, M. H.; Zhao, X.; Chapman, R. Z.; Bender, S. L.; Prevatt, W. D.; Stoykovich, M. P. Charge-Tunable Polymers as Reversible and Recyclable Flocculants for the Dewatering of Microalgae. *Biotechnol. Bioeng.* **2015**, *112*, 74−83.
(47) 't Lam, G. P.; Zegeye, E. K.; Vermue, M. H.; Kleinegris, D. M. M.; Eppink, M. H. M.; Wijffels, R. H.; Olivieri, G. Dosage Effect of Cationic Polymers on the Flocculation Efficiency of the Marine Microalga Neochloris oleoabundans. *Bioresour. Technol.* **2015**, *198*, 797−802.
(48) Liberatore, M. W.; Peterson, B. N.; Nottoli, T.; McCulloch, J. M.; Jinkerson, R. E.; Boyle, N. R.; Posewitz, M. C. Effectiveness of Cationically Modified Cellulose Polymers for Dewatering Algae. *Sep. Sci. Technol.* **2016**, *51*, 892−898.
(49) Israelachvili, J. N. *Intermolecular and Surface Forces*, 2nd ed.; Academic Press: London, 1991.
(50) Liang, H. J. Harvesting Micro Algae. U.S. Patent 9,464,268 B2, 2016.
(51) Hua, D.; Kuang, L.; Liang, H. Self-Directed Reconstitution of Proteorhodopsin with Amphiphilic Block Copolymers Induces the Formation of Hierarchically Ordered Proteopolymer Membrane Arrays. *J. Am. Chem. Soc.* **2011**, *133*, 2354−2357.
(52) Zoppe, J. O.; Ataman, N. C.; Mocny, P.; Wang, J.; Moraes, J.; Klok, H.-A. Surface-Initiated Controlled Radical Polymerization: State-of-the-Art, Opportunities, and Challenges in Surface and Interface Engineering with Polymer Brushes. *Chem. Rev.* **2017**, *117*, 1105−1318.
(53) Szilagyi, I.; Trefalt, G.; Tiraferri, A.; Maroni, P.; Borkovec, M. Polyelectrolyte Adsorption, Interparticle Forces, and Colloidal Aggregation. *Soft Matter* **2014**, *10*, 2479−2502.
(54) Dobrynin, A. V.; Deshkovski, A.; Rubinstein, M. Adsorption of Polyelectrolytes at an Oppositely Charged Surface. *Phys. Rev. Lett.* **2000**, *84*, 3101−3104.
(55) Grenier, D.; Mayrand, D. Functional-Characterization of Extracellular Vesicles Produced by Bacteroides-Gingivalis. *Infect. Immun.* **1987**, *55*, 111−117.
(56) Kamaguchi, A.; Nakayama, K.; Ichiyama, S.; Nakamura, R.; Watanabe, T.; Ohta, M.; Baba, H.; Ohyama, T. Effect of Porphyromonas Gingivalis Vesicles on Coaggregation of Staphylococcus aureus to Oral Microorganisms. *Curr. Microbiol.* **2003**, *47*, 485−491.
(57) Zhang, Z.; Wang, X.; Tam, K. C.; Sèbe, G. A Comparative Study on Grafting Polymers from Cellulose Nanocrystals via Surface-Initiated Atom Transfer Radical Polymerization (ATRP) and Activator Re-Generated by Electron Transfer ATRP. *Carbohydr. Polym.* **2019**, *205*, 322−329.
(58) Jiang, Y.; Zheng, W.; Kuang, L.; Ma, H.; Liang, H. Hydrophilic Phage-Mimicking Membrane Active Antimicrobials Reveal Nanostructure-Dependent Activity and Selectivity. *ACS Infect. Dis.* **2017**, *3*, 676−687.
(59) Li, D.; He, Q.; Yang, Y.; Möhwald, H.; Li, J. Two-Stage pH Response of Poly(4-vinylpyridine) Grafted Gold Nanoparticles. *Macromolecules* **2008**, *41*, 7254−7256.
(60) Arai, K.; Kotaka, T.; Kitano, Y.; Yoshimura, K. Poly(styrene-b-butadiene-b-4-vinylpyridine) 3-Block Polymers - Synthesis, Characterization, Morphology, and Mechanical Properties. *Macromolecules* **1980**, *13*, 1670−1678.
(61) Chang, Y.-P.; Ren, C.-L.; Qu, J.-C.; Chen, X.-G. Preparation and Characterization of Fe_3O_4/Graphene Nanocomposite and Investigation of Its Adsorption Performance for Aniline and P-Chloroaniline. *Appl. Surf. Sci.* **2012**, *261*, 504−509.
(62) Langmuir, I. The Adsorption of Gases on Plane Surfaces of Glass, Mica and Platinum. *J. Am. Chem. Soc.* **1918**, *40*, 1361−1403.
(63) von Werne, T.; Patten, T. E. Atom Transfer Radical Polymerization from Nanoparticles: A Tool for the Preparation of Well-Defined Hybrid Nanostructures and for Understanding the Chemistry of Controlled/"Living" Radical Polymerizations from Surfaces. *J. Am. Chem. Soc.* **2001**, *123*, 7497−7505.
(64) Li, D.; He, Q.; Cui, Y.; Li, J. Fabrication of pH-Responsive Nanocomposites of Gold Nanoparticles/Poly(4-vinylpyridine). *Chem. Mater.* **2007**, *19*, 412−417.
(65) Ohno, K.; Akashi, T.; Huang, Y.; Tsujii, Y. Surface-Initiated Living Radical Polymerization from Narrowly Size-Distributed Silica Nanoparticles of Diameters Less Than 100 nm. *Macromolecules* **2010**, *43*, 8805−8812.
(66) Li, D.; Sheng, X.; Zhao, B. Environmentally Responsive "Hairy" Nanoparticles: Mixed Homopolymer Brushes on Silica Nanoparticles Synthesized by Living Radical Polymerization Techniques. *J. Am. Chem. Soc.* **2005**, *127*, 6248−6256.
(67) Tsarevsky, N. V.; Braunecker, W. A.; Brooks, S. J.; Matyjaszewski, K. Rational Selection of Initiating/Catalytic Systems

DOI: 10.1021/acs.chemmater.9b00336
Chem. Mater. 2019, 31, 4657−4672

for the Copper-Mediated Atom Transfer Radical Polymerization of Basic Monomers in Protic Media: ATRP of 4-Vinylpyridine. *Macromolecules* **2006**, *39*, 6817−6824.
(68) Discher, B. M.; Won, Y. Y.; Ege, D. S.; Lee, J. C. M.; Bates, F. S.; Discher, D. E.; Hammer, D. A. Polymersomes: Tough Vesicles Made from Diblock Copolymers. *Science* **1999**, *284*, 1143−1146.
(69) Li, Y.; Han, D.; Hu, G.; Sommerfeld, M.; Hu, Q. Inhibition of Starch Synthesis Results in Overproduction of Lipids in Chlamydomonas reinhardtii. *Biotechnol. Bioeng.* **2010**, *107*, 258−268.
(70) Simionato, D.; Block, M. A.; La Rocca, N.; Jouhet, J.; Maréchal, E.; Finazzi, G.; Morosinotto, T. The Response of Nannochloropsis gaditana to Nitrogen Starvation Includes De Novo Biosynthesis of Triacylglycerols, a Decrease of Chloroplast Galactolipids, and Reorganization of the Photosynthetic Apparatus. *Eukaryotic Cell* **2013**, *12*, 665−676.
(71) Kosmulski, M. *Chemical Properties of Material Surfaces*, 1st ed.; CRC Press, 2001; pp 88−156.
(72) Toh, P. Y.; Ng, B. W.; Chong, C. H.; Ahmad, A. L.; Yang, J.-W.; Chieh Derek, C. J.; Lim, J. Magnetophoretic Separation of Microalgae: The Role of Nanoparticles and Polymer Binder in Harvesting Biofuel. *RSC Adv.* **2014**, *4*, 4114−4121.
(73) Lee, K.; Lee, S. Y.; Praveenkumar, R.; Kim, B.; Seo, J. Y.; Jeon, S. G.; Na, J.-G.; Park, J.-Y.; Kim, D.-M.; Oh, Y.-K. Repeated Use of Stable Magnetic Flocculant for Efficient Harvest of Oleaginous Chlorella Sp. *Bioresour. Technol.* **2014**, *167*, 284−290.
(74) Lee, K.; Na, J.-G.; Seo, J. Y.; Shim, T. S.; Kim, B.; Praveenkumar, R.; Park, J.-Y.; Oh, Y.-K.; Jeon, S. G. Magnetic-Nanoflocculant-Assisted Water-Nonpolar Solvent Interface Sieve for Microalgae Harvesting. *ACS Appl. Mater. Interfaces* **2015**, *7*, 18336−18343.
(75) Seo, J. Y.; Lee, K.; Lee, S. Y.; Jeon, S. G.; Na, J.-G.; Oh, Y.-K.; Park, S. B. Effect of Barium Ferrite Particle Size on Detachment Efficiency in Magnetophoretic Harvesting of Oleaginous Chlorella Sp. *Bioresour. Technol.* **2014**, *152*, 562−566.
(76) Seo, J. Y.; Praveenkumar, R.; Kim, B.; Seo, J.-C.; Park, J.-Y.; Na, J.-G.; Jeon, S. G.; Park, S. B.; Lee, K.; Oh, Y.-K. Downstream integration of microalgae harvesting and cell disruption by means of cationic surfactant-decorated Fe3O4 nanoparticles. *Green Chem.* **2016**, *18*, 3981−3989.
(77) Prochazkova, G.; Podolova, N.; Safarik, I.; Zachleder, V.; Branyik, T. Physicochemical Approach to Freshwater Microalgae Harvesting with Magnetic Particles. *Colloids Surf., B* **2013**, *112*, 213−218.
(78) Hua, D.; Jiang, J.; Kuang, L.; Jiang, J.; Zheng, W.; Liang, H. Smart Chitosan-Based Stimuli-Responsive Nanocarriers for the Controlled Delivery of Hydrophobic Pharmaceuticals. *Macromolecules* **2011**, *44*, 1298−1302.
(79) Ge, S.; Agbakpe, M.; Zhang, W.; Kuang, L.; Wu, Z.; Wang, X. Recovering Magnetic Fe_3O_4−ZnO Nanocomposites from Algal Biomass Based on Hydrophobicity Shift under UV Irradiation. *ACS Appl. Mater. Interfaces* **2015**, *7*, 11677−11682.
(80) Zhao, H.; Xia, S.; Ma, P. Use of Ionic Liquids as "Green" Solvents for Extractions. *J. Chem. Technol. Biotechnol.* **2005**, *80*, 1089−1096.
(81) Zhu, S.; Wu, Y.; Chen, Q.; Yu, Z.; Wang, C.; Jin, S.; Ding, Y.; Wu, G. Dissolution of Cellulose with Ionic Liquids and Its Application: A Mini-Review. *Green Chem.* **2006**, *8*, 325−327.
(82) Lim, J. K.; Chieh, D. C. J.; Jalak, S. A.; Toh, P. Y.; Yasin, N. H. M.; Ng, B. W.; Ahmad, A. L. Rapid Magnetophoretic Separation of Microalgae. *Small* **2012**, *8*, 1683−1692.
(83) Ge, S.; Agbakpe, M.; Zhang, W.; Kuang, L. Heteroaggregation between PEI-Coated Magnetic Nanoparticles and Algae: Effect of Particle Size on Algal Harvesting Efficiency. *ACS Appl. Mater. Interfaces* **2015**, *7*, 6102−6108.
(84) Hu, Y.-R.; Guo, C.; Wang, F.; Wang, S.-K.; Pan, F.; Liu, C.-Z. Improvement of Microalgae Harvesting by Magnetic Nanocomposites Coated with Polyethylenimine. *Chem. Eng. J.* **2014**, *242*, 341−347.
(85) Wang, S.-K.; Wang, F.; Hu, Y.-R.; Stiles, A. R.; Guo, C.; Liu, C.-Z. Magnetic Flocculant for High Efficiency Harvesting of Microalgal Cells. *ACS Appl. Mater. Interfaces* **2014**, *6*, 109−115.
(86) Dolan, A. K.; Edwards, S. F. Theory of Stabilization of Colloids by Adsorbed Polymer. *Proc. R. Soc. London, A* **1974**, *337*, 509−516.
(87) Scheutjens, J. M. H. M.; Fleer, G. J. Statistical Theory of the Adsorption of Interacting Chain Molecules. 1. Partition Function, Segment Density Distribution, and Adsorption Isotherms. *J. Phys. Chem.* **1979**, *83*, 1619−1635.
(88) Evers, O. A.; Scheutjens, J. M. H. M.; Fleer, G. J. Statistical Thermodynamics of Block Copolymer Adsorption. 1. Formulation of the Model and Results for the Adsorbed Layer Structure. *Macromolecules* **1990**, *23*, 5221−5233.
(89) Fredrickson, G. H. *The Equilibrium Theory of Inhomogeneous Polymers*; Oxford University Press, 2013.
(90) Toh, P. Y.; Ng, B. W.; Ahmad, A. L.; Chieh, D. C. J.; Lim, J. The Role of Particle-to-Cell Interactions in Dictating Nanoparticle Aided Magnetophoretic Separation of Microalgal Cells. *Nanoscale* **2014**, *6*, 12838−12848.
(91) Henderson, R. K.; Parsons, S. A.; Jefferson, B. The Impact of Differing Cell and Algogenic Organic Matter (AOM) Characteristics on the Coagulation and Flotation of Algae. *Water Res.* **2010**, *44*, 3617−3624.

DOI: 10.1021/acs.chemmater.9b00336
Chem. Mater. 2019, 31, 4657−4672